UNIVERSITY OF CALIFORNIA
RIVERSIDE

Exploring the use of MRI Reporters as Therapeutic Agents

A Dissertation submitted in partial satisfaction
of the requirements for the degree of

Doctor of Philosophy

in

Bioengineering

by

Abby Barlow

December 2021

Dissertation Committee:
Dr. Xiaoping Hu, Chairperson
Dr. Joshua Morgan
Dr. B. Hyle Park

Copyright by
Abby Barlow
2021

The Dissertation of Abby Barlow is approved:

_____

_____

_____

Committee Chairperson

University of California, Riverside

ACKNOWLEDGEMENTS

First, I want to thank my advisor, Dr. Xiaoping Hu, for his support and guidance throughout the years which allowed me to develop into an independent researcher. I am also grateful for my co-advisor, Dr. Joshua Morgan, for not only allowing me to perform many experiments in his lab, but his endless guidance and advice that helped make this dissertation possible. I would like to thank my dissertation committee for allowing me to present my research. I deeply value the advice, support, and friendship of my lab mates and fellow graduate students. I also want to give a special thanks to Dr. Jason Langley, Martina Sanchez, and Kaiqing Chen for their help with imaging and creatine experiments. Finally, I would like to thank my friends, family members and especially my Fiancé, Daniel Avenell, for supporting me and helping me get through tough times over the years.

ABSTRACT OF THE DISSERTATION

Exploring the use of MRI Reporters as Therapeutic Agents

by

Abby Barlow

Doctor of Philosophy, Graduate Program in Bioengineering
University of California, Riverside, December 2021
Dr. Xiaoping Hu, Chairperson

Magnetic resonance imaging (MRI) is a non-invasive and non-ionizing imaging modality used to study cellular and molecular events as well as track disease progression in tissues. Due to limited sensitivity, genes, proteins and other molecules can be utilized to increase contrast in specifically labeled tissues and cells for MRI images. MRI reporters are able to provide information on gene expression, cell tracking and migration, and cellular energy metabolism. Additionally, many genes and molecules used to produce contrast may yield therapeutic benefit. Here, we take a closer look at two established MRI reporters: creatine and mms6, and determine their therapeutic potential.

We tested the efficacy of creatine (Cr) supplementation on the brain. Recent studies suggest that Cr supplementation may improve cognitive function and memory, but the major hurdle is bypassing the blood brain barrier. Initially, we developed a creatine nasal spray and hypothesized that we could increase creatine and phosphocreatine (pCr) concentration in mouse brain. Despite multiple rounds of experiments with varying creatine concentration and duration of administrations, we did

not confirm an increase in Cr or pCr in experimental groups. Due to issues resolving Cr and pCr on small tissue samples, we developed a novel pre-incubation technique to convert Cr and pCr to creatinine (Crn) and calculate the concentration of total creatine using commercially available creatine and creatinine assay kits. This technique was demonstrated on Cr and pCr standards as well as mouse muscle and brain tissue.

We tested the ability of MRI reporter *mms6* to enhance gemcitabine cytotoxicity on pancreatic tumor cell line, PANC-1. Mms6 is an iron binding protein found in magnetotactic bacteria. When the *mms6* gene is expressed in mammalian cells, they increase iron uptake and storage producing measurable contrast in T2-weighted MRI images. We created a PANC-mms6 cell line capable of producing MRI contrast, and treated them with a common pancreatic cancer drug, gemcitabine. Given its resistant nature in PANC-1 cells, we hypothesized that we could increase cytotoxicity and cell death in PANC-mms6 cells over non-expressing PANC-WT cells. The results revealed a significant reduction in viability of PANC-mms6 cells after treatment with gemcitabine while PANC-WT cells remained viable under the same conditions.

TABLE OF CONTENTS

LIST OF FIGURES

CHAPTER 1

INTRODUCTION

Magnetic resonance imaging (MRI) is a non-invasive imaging modality that produces measurable contrast by manipulating the magnetic nuclei of molecules within a sample with radiofrequency irradiation inside a magnetic field. This modality can be applied to clinical and research settings for measuring whole tissues and disease progression to detecting cellular and molecular events within a sample. Due to its limited spatial resolution compared to other imaging modalities, genes, proteins and small molecules can be employed to increase contrast for MRI. Reporters already identified and utilized for MRI may hold therapeutic potential for treating the same diseased cells and tissue that are being tracked. The research presented in this dissertation will focus on two MRI reporters for molecular imaging and their potential use as a theranostic agent.

1.1 MRI Basics and Contrast

There are a variety of imaging modalities used for clinical and research settings such as MRI, ultrasound, positron emission tomography (PET), single photon emission computed tomography (SPECT), and x-ray. Each modality provides unique advantages and disadvantages relating to spatial or temporal resolution, non-invasiveness, presence or absence of radiation, etc. MRI is excellent for providing non-invasive deep tissue images without using ionizing radiation, but a major disadvantage is it often lacks

sensitivity. Fortunately, there are ways to combat the sensitivity issue by increasing the magnet strength, targeting different nuclei, or by utilizing reporter genes and contrast agents.

The basic principle of acquiring contrast from an MRI scan is to manipulate the spin of protons subjected to a bulk magnetic field. The difference in composition and water content of tissues allows for distinctive proton spins and therefore produce contrast that can be measured. Various protons can be selected for magnetization measurement; hydrogen (^{1}H) is the most common, while Carbon-13 (^{13}C), Phosphorus-31 (^{31}P), Sodium-23 (^{23}Na), and Fluorine-19 (^{19}F) can also be used. Experiments in the research presented here were performed on a ^{1}H MRI scanner. Within tissues, the higher the water content, the more signal will be produced (Gilad et al., 2008). T1 and T2-

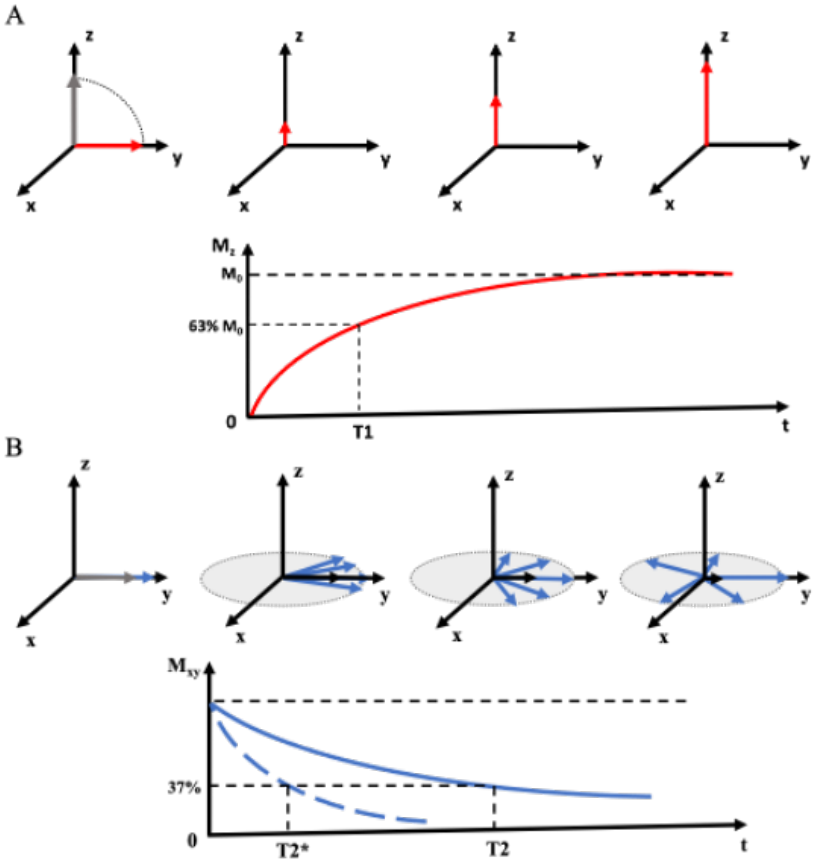

Figure 1: T1 and T2 relaxation in MRI.

weighted contrast is produced and measured based on the relaxation of nuclei after excitation and the dephasing of the nuclei's spin as shown in Figure 1.

The protons in the magnetized nuclei align with the main induced magnetic field, B0. When a radiofrequency pulse is applied, the protons tip out of alignment, then return their alignment to B0. The longitudinal relaxation, or T1 of the proton's tip causes a decrease in signal which can be quantified. This signal can be enhanced by using compounds that further tip the nuclei, such as B-gal or low dose gadolinium (Gilad et al., 2008). While the protons in the excited nuclei are tipping, the phase of their spin is also aligned. The transverse relaxation, or T2, is measured from the dephasing of the protons following demagnetization. A shorter T2 time constant will produce darker contrast in the resulting image. T2* is the T2 measure plus the added effects of magnetic field inhomogeneity. This measurement is taken at 37 percent of the magnetization equilibrium. Enhanced T2 contrast can be produced from iron oxide particles which yields a significant decrease in T2 and T2* time (Gilad et al., 2007; Xiao et al., 2016).

Both two- and three-dimensional data can be obtained from an MRI scanner. For higher spatial and temporal information, an MRI scan is able to provide a three-dimensional image of the subject. Magnetic resonance spectroscopy (MRS) is able to provide only two-dimensional information on the subject but can detect individual proton signals in various metabolites and measure their concentration. This signal is based on the abundance of molecules and interaction with other molecules within the sample.

1.2 MRI Reporter Genes and Contrast Agents

The purpose of reporter genes is to increase contrast and resolution between normal and abnormal tissues. Cellular migration and tracking of labeled cells are also studied using MRI reporter genes. Researcher and clinicians utilize specific genes, proteins, and macromolecules in order to increase contrast in tissues or cells. In molecular MRI, a reporter gene is able to give detailed information about the cell it is expressed in like its location, distribution, and viability. Such genes must also be able to produce contrast under genetic, metabolic, or enzymatic changes. The majority of reporter genes are either iron-based or enzyme-based.

In 1981, the first contrast agent, ferric chloride, was used in a clinical setting for imaging of the gastrointestinal tract. Today, there are many modes of contrast enhancement that can be applied to MRI and MRS. Nearly half of all MRI studies are performed with enhanced contrast using paramagnetic gadolinium compounds or superparamagnetic iron oxide particles. This contrast can be categorized by the following features: chemical composition, presence of metal atoms, route of administration, magnetic properties, and biodistribution (Xiao et al., 2016).

Iron is a paramagnetic reactive metal which is capable of producing its own magnetic signal and local contrast. Compounds like superparamagnetic iron oxide (SPIO) and ultrasmall superparamagnetic iron oxide (USPIO) can be taken up by cells where a reduction in T2 intensity can be observed. Although widely used clinically, a major pitfall of these particles is their lack of ability to produce contrast in dividing cells. Thus,

by integrating iron-binding genes in the host cells, similar particles are produced that owe the same reduction in T2 signal as SPIO and USPIO. Furthermore, these cells are able to continue producing iron oxide nanoparticles through cell division(Elfick et al., 2017, p. 6; Zhang et al., 2014; Zurkiya et al., 2008).

Creatine kinase (CK) was the first MRI reporter gene. CK is an enzyme that catalyzes the conversion of adenosine triphosphate (ATP) and creatine (Cr) into adenosine diphosphate (ADP) and phosphocreatine (pCr). The metabolite phosphocreatine can be detected by ^{31}P MRS while CK is measured by magnetization transfer (CEST imaging) (Menon et al., 2021). This enzyme-based reporter gene has been used in gene expression and energy metabolism related studies (Clark, 1997; Haris et al., 2012). A study done by Li et al. utilized CK to monitor the transfer of low-density lipoprotein receptor (LDLr) gene to hepatocytes in mice (Li et al., 2005). Because there is no expression of CK or any of the creatine metabolites in the liver, CK is a viable reporter for monitoring gene expression. ^{31}P-MRS can give additional information on mitochondrial oxidative metabolism in skeletal muscle by measuring resynthesis of pCr following exercise. Furthermore, creatine metabolites Cr and pCr are widely used as a standard for MRS. Creatine (for MRS, creatine refers to both Cr and pCr) is maintained at a relatively constant level in metabolically active tissues at 3.0 ppm chemical shift and is used as an internal standard. Additionally, the absence of a creatine peak in a cerebral mass may indicate metastasis (Ishimaru et al., 2001).

1.3 Theranostic use of MRI Reporters

Therapeutic agents are defined by their ability to medically treat a disease or condition. Biological agents include chemically synthesized compounds, botanically available molecules, biotherapeutic macromolecules, and nucleic acid-based therapeutics (Kharkar et al., 2017). A theranostic agent has the properties of a therapeutic as well as the diagnostic properties to identify or track disease progression. By unlocking the therapeutic potential of genes and compounds that are already used for enhancing MRI contrast, we can develop robust techniques for diagnosing, tracking, and treatment of various diseases and disorders. The dual therapeutic-reporter technique has been demonstrated on other imaging modalities like ultrasound, optical fluorescence, and positron emission tomography (Guo et al., 2014; Penet et al., 2016; Pruis et al., 2020; Pulsipher et al., 2018). Characterized by the research presented in this thesis, we will be taking a closer look at the therapeutic capacity of MRI reporters: iron-binding magnetobacterial gene, *mms6*, and the creatine metabolites (Cr, pCr, and Creatinine (Crn)).

CHAPTER 2

CREATINE BACKGROUND AND EXPERIMENTAL METHODS

In Chapter 1, we discussed metabolites in the creatine system as reporters for MRS and CEST imaging. Here, we will discuss the background of metabolites within the system, research pertaining to creatine (Cr) and its supplementation, and the inspiration for the studies on Cr supplementation in the brain performed in this lab.

2.1 Creatine Metabolism

Cr is one of the metabolites responsible for high-energy buffering of adenosine triphosphate (ATP) with adenosine diphosphate (ADP) and phosphocreatine (pCr). Cr metabolites are most abundant in tissues with high energy demands such as muscle, brain, and heart (J. T. Brosnan & Brosnan, 2007; Clark, 1997; Harris et al., 1992). Most commonly, bodybuilders supplement with creatine monohydrate or creatine hydrochloride for short intense exercise. In the brain, creatine helps replenish ATP required for rapidly firing neurons and other functions like sodium and calcium transport, intracellular signaling, and support for axons and dendrites (J. T. Brosnan & Brosnan, 2007).

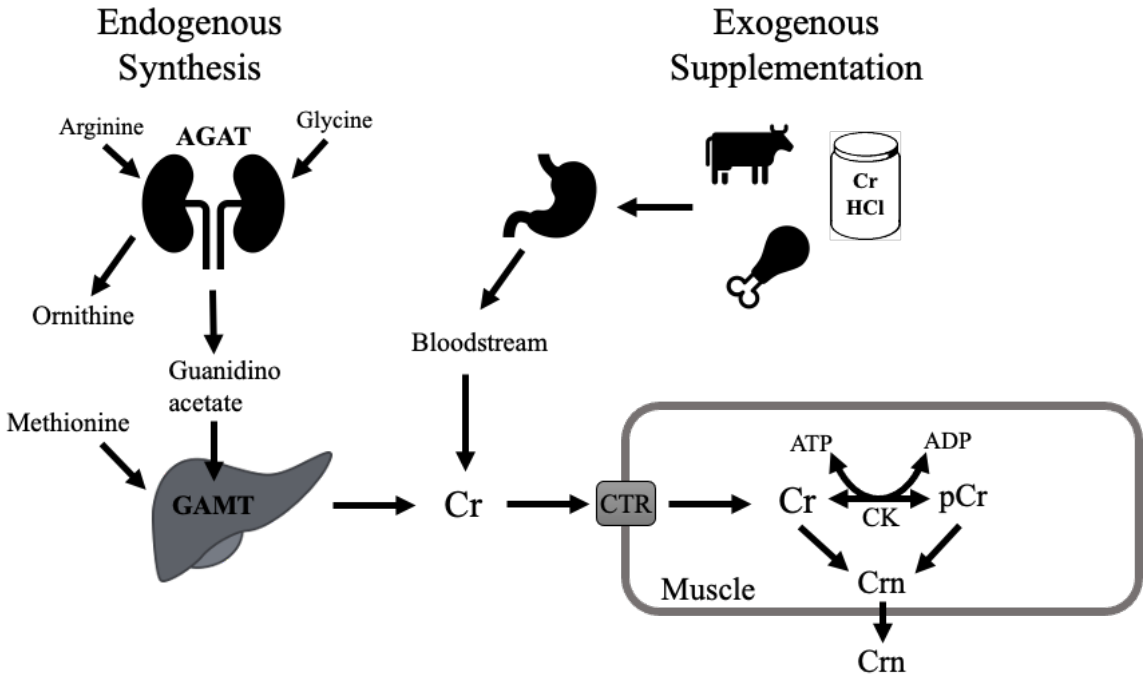

Figure 1: Creatine synthesis, exogenous supplementation, and metabolism in muscle tissue.

The reversible reaction is catalyzed by a single enzyme, creatine kinase (CK), as shown in Figure 1. ADP and pCr are catalyzed into ATP and Cr. Both Cr and pCr are spontaneously converted into their decay product, creatinine (Crn), for excretion through the kidneys (*Borsook: The Hydrolysis of Phosphocreatine and the… - Google Scholar*, n.d.; Meister, 2009). Due to a 1.7% depletion of stores per day, the body must synthesize its own creatine and supplement from diet (J. T. Brosnan & Brosnan, 2007).

Dietary creatine can be found in animal proteins, as well as isolated creatine monohydrate in powder form. In Figure 1, we show how creatine is synthesized in the body. Creatine synthesis begins in the kidney where an amidino group is transferred to the amino group of glycine to produce guanidinoacetate and ornithine. This initial

reaction is catalyzed by L-arginine:glycine amidinotransferase (AGAT). The second reaction is catalyzed by guanidinoacetate methyltransferase (GAMT) in the liver. During this reaction, creatine is produced from S-adenosylmethionine and methylate guanidinoacetate. From here, creatine is distributed to skeletal muscle, heart, and the brain through the bloodstream. Since transport across the blood brain barrier is tightly regulated by creatine transporter (CRT), the brain is capable of synthesizing its own creatine; studies have shown that most brain cells produce AGAT and GAMT enzymes.

As stated before, creatine metabolites can be detected by magnetic resonance. Total creatine (Cr + pCr) can be measured with ^{1}H MRS, though the resolution and long acquisition times make it difficult to measure the metabolites individually in smaller samples. ^{31}P MRS is commonly used to measure ATP and pCr production; this method is more costly and requires a high-intensity magnet (>9.4 Tesla) to resolve Cr and pCr concentrations. Currently, there is no MR method to quantify free Cr separately from pCr at high resolution.

2.2 Prior Research on Creatine

In the nutritional supplement industry, creatine monohydrate has produced over $400 million (Bird, 2003). Since the 1990's, athletes and body builders have experimented with creatine supplementation to improve muscle performance. As it is not a banned substance, its popularity has continued to rise for enhancing athletic performance. PCr is most abundantly stored in skeletal muscle where it can rapidly hydrolyze to release ATP for immediate energy use. PCr stores are limited and therefore

can only sustain about 5 to 10 seconds of intense exercise before needing replenishment (Bird, 2003). Kurosawa et al. performed a study comparing the rate of ATP synthesis and pCr hydrolysis. They found that a daily dose of 30 g creatine monohydrate for 14 days was able to increase ATP synthesis and mean power output during short, intense exercise (Bird, 2003). Similar studies are in support that supplementation with creatine is able to increase intramuscular stores of pCr (Harris et al., 1992; McKenna et al., 1999; Stout et al., 2001; Vandenberghe et al., 1997). PCr utilization and depletion is almost exclusively reliant on intensity and duration of energy.

Failure to produce or supplement a sufficient amount creatine results in various maladies. Gyrate atrophy is characterized by degeneration and atrophy of type 2 muscle fibers. Due to mutations in ornithine aminotransferase and AGAT enzyme, creatine synthesis is inhibited. Other muscular creatine related abnormalities include McArdle's disease and Duchenne muscular dystrophy (Persky & Brazeau, 2001). Creatine supplementation is able to reduce and eliminate muscle deformities (J. T. Brosnan & Brosnan, 2007).

When creatine and phosphocreatine are not sufficiently produced or supplied to the brain, neurological disorders arise. Inborn errors of creatine synthesis are generally caused by insufficient production of creatine precursors AGAT or GAMT, or creatine transporter CRT. GAMT and CRT deficiencies result in depleted Cr and pCr stores in the brain leading to mental retardation, speech delay, and epileptic seizures (Mercimek-Andrews & Salomons, 1993). Although oral supplementation with creatine can replenish

stores in muscles, the tightly controlled blood brain barrier does not allow excess creatine to pass through. Because of this issue, many researchers have studied alternate routes of creatine supplementation for neurological disorders with mixed results (Matthews et al., 1999).

Apart from treatment of neurological disorders, there has been interest in studying the role of creatine supplementation and brain energetics in healthy individuals. It is hypothesized that by increasing the pCr stores in the brain, it is possible to improve brain functions like cognition and memory (Avgerinos et al., 2018; Pan & Takahashi, 2007). Neurons require energy to carry out multiple processes. CRT is most abundant in areas of the brain such as the olfactory bulb, hippocampus, cerebral cortex, cerebellum, brain stem and spinal cord (Pan & Takahashi, 2007). Consequently, many of these regions that express higher levels of CRT are compromised in Alzheimer's disease, Huntington's disease, and other psychiatric disorders. Avgerinos et al. performed an analysis of six studies that explored creatine supplementation and its effects on cognition, memory, executive function, and intelligence and reasoning (Avgerinos et al., 2018). Improvements in function were revealed in studies pertaining to short and long-term memory, response inhibition, and intelligence (reasoning/mathematical processing). Due to the varying success of other research studies on creatine supplementation for the brain, we decided to explore the nasal route as a method of creatine delivery in order to bypass the issue of the blood brain barrier.

2.3 Nasal Delivery of Creatine in Rodents

Our initial creatine study explored the nasal delivery of creatine in rodents to increase creatine within the brain for cognition and energetics experiments. Since CRTs at the blood brain barrier tightly control the amount of creatine allowed to pass through, the therapeutic potential of oral creatine is limited for neurological diseases (Allen, 2012). We hypothesized that we could increase Cr and pCr levels in the brain by administering creatine supplement through the nasal passage. To bypass the blood brain barrier, we formulated a nasal spray to deliver creatine to mouse and rat brain. Various concentrations and nasal administration time points were tested in order to measure an increase in Cr, pCr, and total creatine (Cr + pCr) within the brain.

We set up 5 rounds of experiments with 8-12 mice in each round split into creatine administered and control groups. We began the first round by administering a single dose of 2.5 mg (100 mg/kg body weight) of creatine HCl dissolved in PBS. After sacrifice and harvesting brain the brain tissue, we did not see any difference in creatine concentration between the experimental and control group. We repeated the experiment with a lower volume of creatine solution and got similar results. For the next 3 rounds of experiments, we increased the concentration to 5 mg and 7 mg doses and increased the duration of administration to 5 days and finally, 4 weeks. Still, the results did not show an increase in creatine within the brain.

We concluded the study without any positive results from the initial experiments: creatine concentration of treated mice for 4 rounds of treatment showed a fold change of 1.01 +/- 0.55, 0.927 +/- 0.11, 0.869 +/- 0.35, and 0.836 +/- 0.14 compared to untreated mice. Perhaps moving to human subjects would allow us to scan the larger subjects and confirm proper nasal insufflation. However, through trouble shooting and optimizing creatine measurement techniques, we were able to develop a benchtop preincubation technique for capturing total creatine within a sample. A necessity for this technique came about when we needed a way to confirm creatine and phosphocreatine concentrations in the brain samples. As stated earlier, ^{1}H 3T MRI has a lower resolution and it is difficult to resolve Cr and pCr using MRS on small mouse brain samples. In the next chapter, we will discuss the preincubation technique developed to measure total creatine in a biological sample.

2.4 Experimental Methods

Animal Use

All procedures were conducted in accordance with the National Institutes of Health guidelines and approved by the Institutional Care and Use of Laboratory Animals committee at the University of California, Riverside. We purchased 3-week old C57Cl/6 wild-type mice from Jackson Laboratories (Catalog #: 000664) for our initial studies on nasal delivery of creatine. In order to test the pre-incubation technique described in Chapter 3, we were gifted muscle and brain tissue post-mortem from C57Bl/6 mice provided by Dr. Ansel Hsiao (University of California, Riverside, Riverside, CA, USA).

All mice were kept on a 12-hour light/dark cycle with unrestricted access to standard food and water.

Nasal Spray Solution

For the initial experiments in this study, we formulated a nasal spray composed of creatine hydrochloride (HCl) and phosphate buffered saline (PBS). Creatine dose of 100 mg/kg body weight was calculated depending on the weight of the mice. The creatine powder was dissolved in PBS. The nasal spray was made fresh and kept sterile for each experiment. The spray was administered by pipette into the nasal passage of anesthetized mice. For each experiment, 3 mice were used as controls and 3 mice were administered creatine. Total creatine administered per day to the experimental group and duration of daily administrations varied across 5 experiments. The experimental groups received 2.5, 5, or 7 mg per day for 1-5 day and 4-week time points.

Dissection and Tissue Preparation

All mice were deeply anesthetized with isofluorane (Henry Schein, Pasadena, CA, USA) prior to sacrifice by decapitation. Immediately after sacrifice, brain and skeletal muscle tissues were harvested and snap frozen by submersion in liquid nitrogen. To prepare tissues for creatine and creatinine assays, we homogenized each tissue in PBS using a dounce homogenizer.

Creatine, Phosphocreatine, and Creatinine Standard Preparation

In order to test the proposed method of converting creatine and phosphocreatine to creatine for total measurement of metabolites, we prepared standard solutions of creatine, phosphocreatine, and creatinine. Creatine HCl (GNC) was used to create the creatine standard by dissolving the powder in diH_2O to a concentration of 1000 μM. Phosphocreatine disodium salt (Sigma Aldrich, St. Louis, MO, USA) was dissolved in diH_2O also at a concentration of 1000 μM. Creatinine standard was obtained from the bioassay systems creatinine assay kit and diluted to 1000 μM as well. Samples were prepared fresh for every experiment.

Creatine and Creatinine Assays

To measure only creatine in the samples, we used an enzymatic creatine assay from Sigma Aldrich (catalog #: MAK079). Homogenized samples were assayed directly. For measuring initial creatinine and post-converted total creatine samples, we used an enzymatic creatinine detection kit for tissues and a Jaffe-related biochemical assay kit (BioAssay Systems, Hayward, CA, USA) for creatine standard experiments. The absorbance was detected at 570 nm with a Molecular Devices SpectraMax M2 microplate reader.

Statistics

For rat tissue comparisons, there were 3 rats used for each treatment group. Each sample was assayed in triplicate. Statistics were performed using Microsoft Excel and MATLAB. Student's t-tests were performed on creatinine data using mean values and

standard error of tissues pre- and post-processed. Differences were considered significant at * $p<0.05$, ** $p<0.01$, and *** $p<0.001$ levels.

CHAPTER 3

A PREINCUBATION TECHNIQUE FOR A SIMPLIFIED MEASUREMENT OF TOTAL CREATINE

3.1 Introduction

Creatine (Cr) and its stored form, phosphocreatine (pCr), are naturally occurring metabolites mainly found in metabolically active tissues with a fluctuating energy demand such as muscle, brain, and heart (Turner & Gant, 2014). Cr metabolites are crucial for buffering, transporting, and regulating cellular energy. Phosphocreatine is especially critical in maintaining low adenosine diphosphate levels and the transfer of high energy phosphate from the mitochondria (M. E. Brosnan & Brosnan, 2016). Although the body is capable of synthesizing its own creatine, it may also be obtained through diet. Every day, approximately 2% of creatine and phosphocreatine spontaneously degrade into creatinine which is then excreted through the kidney. Creatine and phosphocreatine are most commonly associated with exercise and muscle studies (M. E. Brosnan & Brosnan, 2016; Clark, 1997). These compounds have also been reported as potential markers for endotoxin shock, cellular damage due to shock and ischemia (Jabs et al., 1988). Creatinine is the most commonly measured urinary metabolite for determining glomerular filtration rate (Peake & Whiting, 2006).

Creatinine was first measured in 1886 when the Jaffe method was developed by observing the properties of creatinine in the presence of picric acid in an alkaline solution (Beard, 1941; Jaffe, 1886; Peake & Whiting, 2006). For nearly a century, most assays developed for measuring creatine compounds were adapted from the Jaffe reaction (Peake

& Whiting, 2006). Although the method is quick and cost-effective, the use of picric acid can be dangerous as it is an extremely acidic phenol and is explosive (Akhavan, 2011). Further, employing the method requires careful control of reaction temperature and it is not particularly useful for quantifying both creatine and phosphocreatine. Enzymatic methods began to emerge in the latter half of the 20th century and are commonly available for measuring creatine and creatinine, but not phosphocreatine. These methods are simple and effective but insufficient for measuring the full range of creatine compounds (Sellevold et al., 1986).

Near the end of the 20th century, high-performance liquid chromatography (HPLC) emerged as a novel method for measuring creatine compounds. With increased accuracy and sensitivity by directly determining the mass of metabolites, HPLC is superior to its biochemical assay counterparts (Sun et al., 2019). While it is not a new technique, HPLC requires expensive capital investment, running costs and trained personnel. Further, HPLC is a time-consuming process; it requires additional time for pretreatment and regeneration of the column after each run (Sellevold et al., 1986; Sun et al., 2019). Because of the high operating costs and training, this method is not always practical for small labs and experiments.

^{31}P nuclear magnetic resonance (NMR) and ^{1}H magnetic resonance spectroscopy (MRS) were developed in the 1970s with the ability to measure creatine compounds. Like HPLC, they involve large capital and running expenses. Further, common 1.5-2 T NMR magnets require long scanning durations and provides limited spatial resolution, making MRS a poor choice for rodents or other small subjects (Ladd et al., 2018).

3.2 Methods/Results

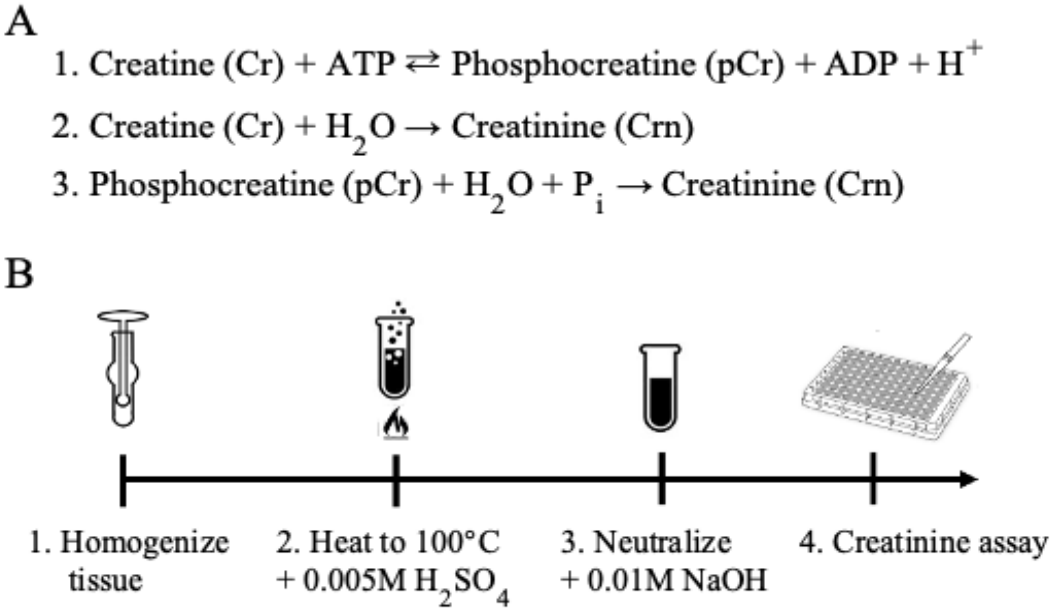

Figure 3: Schematic of pre-incubation technique. A) Chemical equations for creatine (Cr), phosphocreatine (pCr), and creatinine (Crn). B) Four-step process for converting Cr and pCr into Crn for total measurement.

To provide and accessible and cost-effective method, we chemically convert all species to creatinine through heat with an acid catalyst. Through measurement of the samples before and after treatment, creatinine (Crn) and creatine (Cr) can be measured using readily available kits while phosphocreatine can be inferred. The creatine molecule has a half-life of 3 hours and prefers to be in its phosphorylated state (pCr) (Vanakoski et al., n.d.). Unfortunately, there are no readily available kits for directly measuring

phosphocreatine in a tissue sample. To address this, we developed our own method (Figure 1). For this method, tissues can be directly homogenized with phosphate-buffered saline (PBS) or sterile water. Sulfuric acid (0.005 M) is used to acidify the solution to a pH of 2. By heating the solution to 90-100 °C) the Cr and pCr within the sample will convert to their end state, Crn. The stoichiometric ratio is 1:1 for both conversions within the sample, allowing for the ready calculation of total creatine (Cr + pCr) through Crn measurements. Additionally, since Crn is a commonly measured diagnostic for renal/urinary function, assay kits for detecting creatinine are readily and cheaply available.

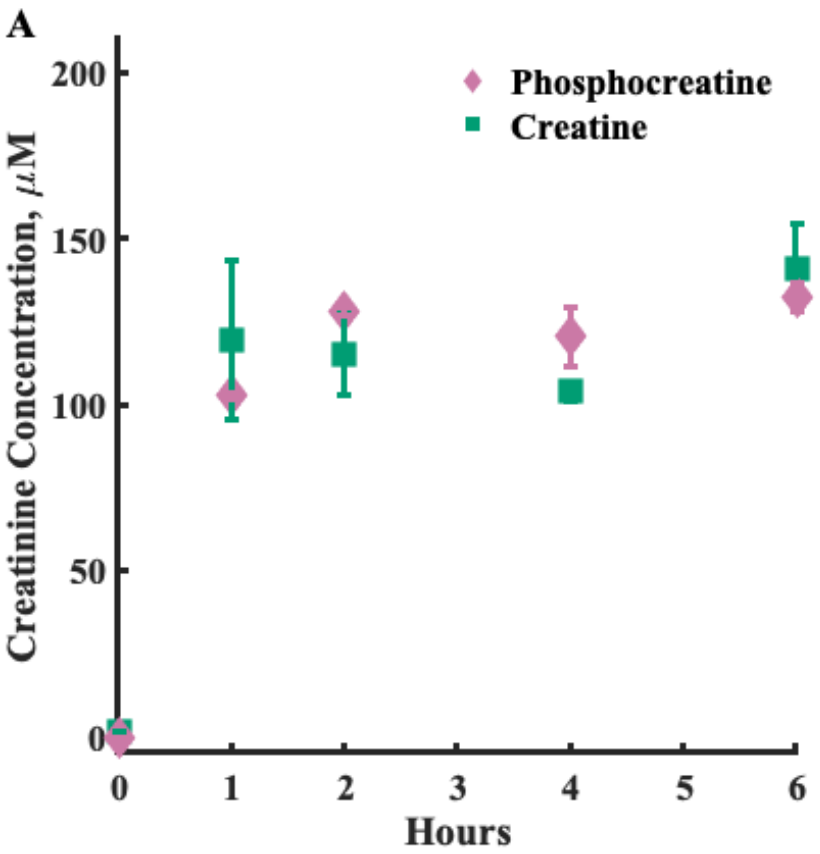

Figure 4: Creatinine concentration of Cr (green) and pCr (pink) after incubation for 0, 1, 2, 4, and 6 hours. Creatinine standards were used to normalize Cr and pCr measurements All samples and standards were run in triplicate.

First, we tested the technique by loading samples of known concentration for Cr, pCr, and Crn. Creatine HCl (GNC) and phosphocreatine disodium salt (Sigma Aldrich) powders were used for creatine and phosphocreatine controls,

respectively. Each powder was measured and diluted in sterile water to obtain a starting concentration of 1000 µM. Creatinine standard (BioAssay Systems) was also diluted to 1000 µM in sterile water. 400 µl of sulfuric acid was added to 100 µl of sample, bringing the total concentration of sample down to 200 µM. The rates of decay were plotted for Cr and pCr (Figure 2A) with Crn as the standard. The time to completion for creatine and phosphocreatine compounds is approximately 4-6 hours.

To determine the feasibility of the proposed method on *ex vivo* tissue, we conducted experiments on muscle and brain tissues harvested from 3 wild-type Black/6 mice acquired post-mortem. Animals were euthanized for reasons unrelated to the study.

The brain and muscle tissues were harvested and immediately homogenized with equal volume diH_2O then kept on ice. Similar to the control experiments, 400 µl of 0.005M sulfuric acid was added to 100 µl of homogenized sample. Figure 3 shows the measured

Crn in the tissues before (yellow) and after (green) the pre-incubation conversion technique. Due to the 1:1 stoichiometry of creatine metabolites to Crn, we can estimate total creatine based on post-conversion Crn concentration (pink). Muscle contains the highest concentration of Cr and pCr in the body and has a reported physiological range of 22-42 µmol total creatine per gram of tissue (Chanutin, 1927; Miller et al., 1939; Rose et al., 1927). Here, we measured an average of 6 µmol/g tissue before treating the samples, and about 18.3 µmol/g tissue post conversion treatment (n=3), which is slightly below previously reported range. Students T-test results comparing pre- to post-processed muscle tissue showed a p-value of 0.0611. The brain is the second most concentrated tissue at 8.2-17 µmol/g tissue (Chanutin, 1927; Miller et al., 1939). We measured an average of 2.81 µmol/g tissue before

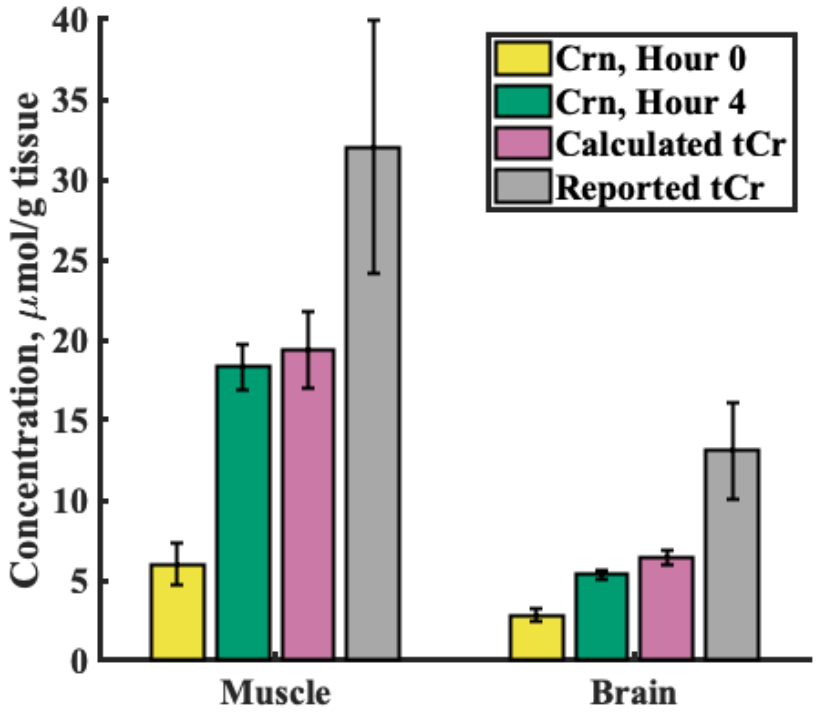

Figure 5. Brain and muscle tissue measured before and after preincubation technique. Initial creatinine concentration is shown in yellow, creatinine measured after 4 hours in green, calculated total creatine in pink, and reported physiological range is in gray. N = 3, samples were measured in triplicate.

treating the samples, and about 5.39 μmol/g tissue post conversion treatment (n=3), about half of reported range concentration. A student's T-test performed on pre- vs post-processed tissue showed a significant difference (p-value of 0.0003).

3.3 Discussion

The method described here can improve current benchtop techniques to quantify all three creatine metabolites (phosphocreatine, creatine, and creatinine) in various tissues. This technique is simple, cost-effective, and functions well for physiological concentrations of interest in the brain and muscle. Furthermore, if one wants to determine the ratio of Cr to pCr, the untreated, homogenized sample can be easily measured by commercially available Cr assays and compared with the total creatine concentration. This is appropriate for labs studying metabolism and metabolic disorders and do not have ready access to HPLC or MRS.

CHAPTER FOUR

REPORTER GENE BACKGROUND AND EXPERIMENTAL METHODS

A number of different iron-related MRI reporter genes have been identified from magnetotactic bacteria. The *mms6* gene has so far been isolated and employed in research on 9L rat gliosarcoma and human mesenchymal stem cell lines (Elfick et al., 2017; Zhang et al., 2014). In this chapter, we will discuss the origin, previous studies, and potential for treatment of pancreatic cancer in combination with gemcitabine.

4.1 Magnetotactic Bacteria

Magnetotactic bacteria are unique as they are able to sense the earth's magnetic field. These special bacteria are gram negative, microaerophilic organisms that live and move about in an aquatic environment (Blakemore, 1975). They are motile by use of magnetotaxis to influence swimming direction to a more or less oxygen rich environment. Most common strains of Magnetotactic bacteria include: MSR-1, AMB-1, MS-1, and MC-1 (Richter et al., 2007).

In order to align themselves with the magnetic field, these bacteria internally produce strands of magnetic nanoparticles that act as a compass. These nanoparticles are referred to as magnetosomes; they are made of either magnetite (Fe_3O_4) or greigite (Fe_3S_4) and are enclosed within a lipid bilayer. Researchers have been able to identify a region of the bacterial genome that contains most genes required for magnetosome formation (Murat et al., 2010; Nudelman et al., 2018; Richter et al., 2007). The region is known as the

magnetosome island (MAI). Studies have shown that MAI loss or removal results in a nonmagnetic phenotype, indicating its importance for magnetosome formation. Sections of the MAI are essential for different roles, performed in a step-wise manner for complete magnetosome formation and stabilization. These roles include magnetosome membrane biogenesis, magnetosome protein localization, and biomineralization. As it is a complex process, multiple factors are essential for crystal formation including size, number, and morphology (Richter et al., 2007).

4.2 Mms6 as a Reporter for MRI

Magnetic particle membrane specific 6 or *mms6* is a 402 bp gene located in the MAI that encodes a protein crucial for magnetite nucleation and crystal growth. Proteins within the same region express motifs that interact with iron and the magnetite surface (Nudelman et al., 2018). The mms6 protein is amphipathic and is composed of a hydrophobic N-terminal domain and hydrophilic C-terminal (Zhang 2014). When Fe^{2+} is present in the cell environment, mms6 is able to promote formation and morphology of superparamagnetic nanoparticles *in vivo* and *in vitro*. Furthermore, deletion of this gene in magnetotactic bacteria results in defects of magnetite size and shape (Nudelman et al., 2018).

Recent studies have explored the use of *mms6* in 9L rat gliosarcoma and human mesenchymal stem cells. Zhang et al stably expressed *mms6* in the 9L cancer cell line and examined its potential as a reporter for MRI *in vitro* and *in vivo*. Significant contrast was produced in cells incubated with ferric citrate as well as inoculated tumors in rat hindleg

(Zhang et al., 2014). In another study, Elfick et al used the *mms6* gene to target and track therapeutic stem cells. After gaining stable transfection of mms6 in mesenchymal stem cells, they were able to track parent cells as well as daughter cells resulting from division (Elfick et al., 2017). This is a major advantage for tracking specifically labeled cells without the need to add more contrast since these cells are able to produce their own local contrast from endogenous iron stores.

4.3 Iron and Gemcitabine in Cancer Therapy

In the next chapter, we will be discussing the enhanced effect of gemcitabine (GEM) on PANC-1 cells engineered with the *mms6* gene. There have been a few studies on the effect of iron manipulation with gemcitabine treatment for pancreatic and other cancer types (Amano et al., 2020; Khan et al., 2019; Kush et al., 2020; Shinoda et al., 2018).

All cells require iron for cell growth and proliferation. Iron deficiency can lead to anemia through cell growth arrest and death (Sherman et al., 2018). Its chemical properties as a transition metal are unique important to cellular function. Ferric (Fe3+) iron is reduced to ferrous (2+) before it is transported across the cell membrane. From there, it is either used or stored within the cell. The Fenton reaction that is produced from the ferrous iron reacting with hydrogen peroxide (H_2O_2) is toxic to cells. The free radicals produced from the reaction can damage lipid membranes, proteins, and nucleic acids, which leads to cell death (Hentze et al., 2004). Too much or too little iron can lead to cell death; therefore, it is crucial for iron levels to be controlled and limited.

GEM is a nucleoside analog of deoxycytidine most commonly used for treating pancreatic cancer. Cytotoxicity occurs after exertion of inhibitory actions on DNA synthesis. Although GEM treatment is more effective than other chemotherapy drugs like fluorouracil, doxorubicin, and cisplatin, it still has limited capacity when used by itself on pancreatic cancer. The need for a secondary therapeutic technique stems from the tumor-resistant behavior and short half-life of GEM. Researchers have developed dual-drug techniques to reduce GEM resistance and overall concentration needed to induce cytotoxic effects in tumors (Khan et al., 2019; Qiao et al., 2016; Shinoda et al., 2018). GEM resistance can occur due to various extrinsic and intrinsic mechanisms. Defective human concentrative nucleoside transporter 1 (hCNT1), and downstream converting enzymes ribonucleotide reductase M1 (RRM1), M2 (RRM2) and deoxycytidine kinase (DCK) can contribute to GEM resistance. In the work presented in this thesis, we will take a closer look at human RRM1 and RRM2 in response to gemcitabine in our magnetically engineered cells.

4.4 Experimental Methods

Cell Culturing

We performed all experiments in Chapter 5 on a pancreatic cancer cell line, PANC-1 (ATCC, Rockville, MD, USA). Capable of producing tumors, PANC-1 is an epithelial cell line that can adhere to cell culture treated flasks. Cells were cultured in 100-millimeter cell culture treated plates containing 10 mL of cell culture medium. Cell

culture media was composed of Dulbecco's Modified Eagle's Medium (DMEM) supplemented with 10% fetal bovine serum (FBS) and 1% penicillin and streptomycin. According to the manufacturer, trace amounts of ferric nitrate (0.1 mM) are contained in DMEM (ATCC). Cells were grown at 37 degrees Celsius under 5% carbon dioxide (CO_2) conditions in an incubator. For stable selection and culturing, 2 µg of puromycin was supplemented for each ml of media.

Molecular Cloning

The mms6 gene was isolated from *Magnetospirillum magneticum* strain AMB-1 and optimized for mammalian expression. The accession number for *mms6* is NCBI Reference Sequence NC_007626.1. The pTwist-mms6 plasmid was produced with the 402 bp mms6 gene inserted into a lenti-viral vector (pTwist Lenti SFFV Puro WPRE) and synthesized through commercial vendor Twist Bioscience (Appendix A). First, lentivirus was generated in 293T cells by co-transfecting pTwist_mms6 with packaging plasmids psPAX2 and pMD2G. Cell culture media was collected 48 hours post-transfection, and resulting virus was used to infect PANC-1 cells. After infection and stable selection for 2 weeks using puromycin, the PANC-mms6 cell line was established and used for all experiments in Chapter 5.

RT- and qPCR Analysis

Following the manufacturer's instructions, total RNA was isolated from PANC-WT and PANC-mms6 cells using the Isolate II RNA mini kit (Meridian Bioscence, Memphis,

Tennessee, USA). Complementary DNA was synthesized and quantified using the SensiFast no-ROX SYBR-Green master mix (Meridian Bioscence, Memphis, Tennessee, USA) on a micPCR thermocycler. Forward and reverse primers used for mms6 expression were 5'- GCCGCCGCAATGGGAGAAATGGAAA-3' and 5'-TTAAGCGAGGGCATCCCGCAACT-3', respectively. For the RT-PCR experiment on mms6 expression, the resulting PCR product was separated by electrophoresis and resolved on a 2% w/v agarose gel and imaged. qRT-PCR was also performed on PANC-mms6 and PANC-WT cells to compare hRRM1 and hRRM2 expression. Primers obtained from IDT used for hRRM1 include forward primer: 5'-AAAGGAAGAGCAGCGTGCCAGA-3' and reverse primer 5'-ACCTCATCCAGACCAGGACACT-3'. For hRRM2, primers include 5'-CTGGCTCAAGAAACGAGGACTG-3' (forward) and 5'-CTCTCCTCCGATGGTTTGTGTAC-3' (reverse). Glyceraldehyde 3-phosphate dehydrogenase (GAPDH) was used as a housekeeping gene. The relative amount of mRNA compared with GAPDH level was calculated using crossing point (Cp) values. Results of gene expression were plotted compared to control.

In Vitro Imaging

PANC-mms6 and PANC-WT cells were cultured in media containing 0, 100, and 200 μM iron for 48 hours. ~10^7 cells were then trypsinized, collected in 0.6 ml microcentrifuge tubes, and allowed to settle by gravity for 2 hours. Pellets were imaged using a Siemens 3T Trio MR scanner. T2 and R2 (R2 = 1/T2) were calculated by fitting

decay curves produced from a Carr-Purcell-Meiboom-Gill (CPMG) sequence. Imaging parameters: TE = 20–400 ms in increments of 20 ms, TR = 1500 ms, FOV = 128 × 128 mm, in-plane resolution = 0.5 mm, and a slice thickness = 1 mm. Image processing and analysis were performed using MATLAB and Excel.

MTT Assay

12-well plates were seeded at a density of 10^6 cells per well with either PANC-WT or PANC-mms6 cells. Cells were treated with vary concentrations of iron (0, 10, 50, and 100 μM) and gemcitabine (0, 20, 50, and 100 μM) then cultured for 48 hours. MTT assay reagent and serum free media was added to the cells at a final concentration of 2.5 mg/mL. Cells were then incubated at 37°C with 5% CO_2 for 4 hours. The medium was removed and 100 μL of DMSO was added to each well. The plate was placed on a shaker for 10 minutes to allow all precipitate to dissolve. The absorbance was detected at 570 nm with a Molecular Devices SpectraMax M2 microplate reader.

Live/Dead Assay

PANC-mms6 and PANC-WT cells were cultured in 35 mm cell culture plates with media supplemented with 50 μM iron and 50 μM gemcitabine for 0-, 24- and 48-hour time points. Untreated PANC-mms6 and PANC-WT cells were used as a control. 2 drops of NucBlue® Live reagent (Hoechst 33342) and NucGreen® Dead reagent were added to each well of cells. The cells were incubated at 37°C with 5% CO_2 for 10 minutes then imaged using a Leica SPEII confocal microscope.

Statistics

For MRI scans, there were 3 plates of cells used for each treatment group. Each sample was assayed in triplicate. Statistics were performed using Microsoft Excel and MATLAB. Student's t-tests were performed on MRI R2 data and qPCR data using mean values and standard error. Chi-squared tests were performed on MTT data for 0 fe, 10 fe, and 50 fe groups. Differences were considered significant at * $p<0.05$, ** $p<0.01$, and *** $p<0.001$ levels.

CHAPTER 5

BACTERIAL GENE AND MRI REPORTER, MMS6, ENHANCES GEMCITABINE THERAPEUTIC RESPONSE IN PANCREATIC CANCER

5.1 Introduction

Pancreatic cancer is predicted to rise from the 4th to the 2nd most common cause of cancer-related mortality in the United States by 2030 (McGuigan et al., 2018). Being highly aggressive and difficult to detect early on, pancreatic cancer has a relative 5-year survival rate of less than 5% (Qiao et al., 2016). Surgical resection is currently the only potential cure; however, due to non-specific symptoms and close proximity to major blood vessels, 80% of tumors are not resectable by the time they are detected (McGuigan et al., 2018; Qiao et al., 2016).

Gemcitabine (GEM) is the standard chemotherapeutic agent for treating pancreatic cancer that is approved by the Food and Drug Administration (Qiao 2016). GEM is a prodrug that exerts antitumor activity through inhibition of DNA synthesis, leading to chain termination, DNA fragmentation, and cell death {Citation}. Although it has more significant clinical benefit than fluorouracil, GEM has a short half-life *in vivo* and requires a larger dose posing a greater risk of side effects (Qiao et al., 2016). In recent years, researchers have studied effects of combination chemotherapies with GEM including fluorouracil, leucovorin, oxaliplatin, and irinotecan (Shinoda et al., 2018). These combination therapies show therapeutic advantage over GEM-only treatment, still they also present a higher incidence of side effects (Shinoda et al., 2018).

mms6 is a gene found in magnetotactic bacteria strain AMB-1; it plays a dominant role in magnetosome crystal size and morphology. Recent studies have shown that when this gene is integrated into a mammalian cell genome, the cells increase uptake of endogenous iron and produce their own iron oxide nanoparticles (Figure 1A)(Zhang et al., 2014). Due to the ability to manipulate T2/T2* signal, *mms6* has proven to be a potential reporter for magnetic resonance imaging (MRI) by providing local endogenous contrast that can be passed on to cell progeny (Zhang et al., 2014).

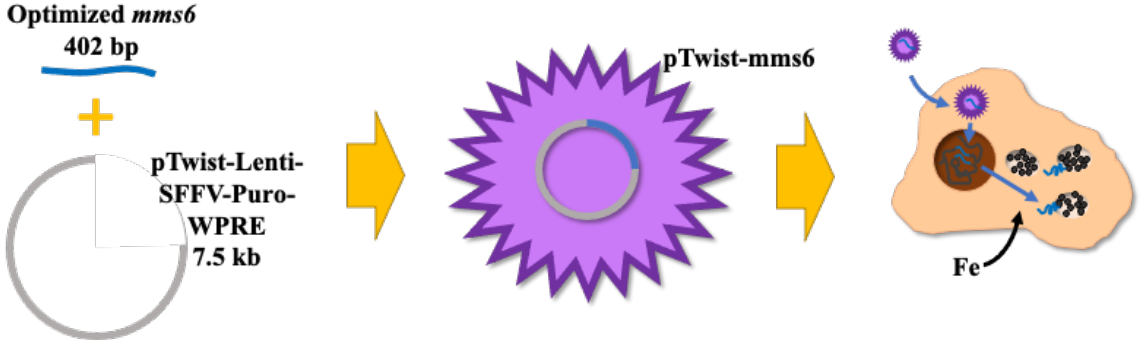

Figure 6: Schematic of viral transduction and iron uptake in PANC-1 cells.

In this study, we stably transfected in Human Pancreatic Carcinoma (PANC-1) cells with the gene, *mms6*; we then investigated its use as an MRI reporter as well as its ability to enhance GEM induced cell death.

5.2 Materials and Methods

Cell line and cell culture. The human pancreatic cancer cell line PANC-1 was used for this study. PANC-1 cells were cultured in Dulbecco's modified Eagle's medium (DMEM) supplemented with 10% fetal bovine serum and 1% Penicillin/Streptomycin at

37°C with 5% CO_2. For the experimental groups, varying concentrations of iron (Ferric Citrate, Sigma Aldrich) and/or varying concentrations of gemcitabine were supplemented to PANC-1 media.

mms6 Expression Vector and Viral Transduction. Expression vector pTwist_mms6 was obtained through Twist Biosciences by modifying *mms6* to fit a mammalian expression system and inserted into a lenti-viral plasmid (pTwist Lenti SFFV Puro WPRE). Lentivirus was generated in 293T cells by co-transfecting pTwist_mms6 with packaging plasmids psPAX2 and pMD2G. Cell culture media was collected 48 hours post-transfection, and resulting virus was used to infect PANC-1 cells. Resulting cells, PANC-mms6, were used as the experimental group in this study. PANC-mms6 cells were passaged several times with regular culture media supplemented with 2 ug/ml puromycin to obtain a stable line. Control cells were referred to as PANC-WT in all experiments.

MRI of cells in culture. PANC-mms6 and PANC-WT cells were cultured in media containing 0, 100, and 200 μM iron for 48 hours. ~10^7 cells were then trypsinized, collected in 0.6 ml microcentrifuge tubes, and allowed to settle by gravity for 2 hours. Pellets were imaged using a Siemens 3T Trio MR scanner. T2 and R2 (R2 = 1/T2) were calculated by fitting decay curves produced from a Carr-Purcell-Meiboom-Gill (CPMG) sequence. Imaging parameters: TE = 20–400 ms in increments of 20 ms, TR = 1500 ms, FOV = 128 × 128 mm, in-plane resolution = 0.5 mm, and a slice thickness = 1 mm. Image processing and analysis were performed using MATLAB and Excel.

Cytotoxicity Assays. 12-well plates were seeded at a density of 10^6 cells per well with either PANC-WT or PANC-mms6 cells. Another transgenic cell line PANC-pCDH-Gli1-Clover was also used as a secondary control. Cells were treated with vary concentrations of iron (0, 10, 50, and 100 μM) and gemcitabine (0, 20, 50, and 100 μM) then cultured for 48 hours. MTT assay and serum free media was added to the cells at a final concentration of 2.5 mg/mL. Cells were then incubated at 37°C with 5% CO_2 for 4 hours. The medium was removed and 100 μL of DMSO was added to each well. The plate was placed on a shaker for 10 minutes to allow all precipitate to dissolve. The absorbance was detected at 570 nm with a Molecular Devices SpectraMax M2 microplate reader. Subsequently, a live/dead assay was performed on PANC-WT and PANC-mms6 cells with and without supplementation of 50 μM iron and 50 μM gemcitabine. 2 drops of NucBlue® Live reagent (Hoechst 33342) and NucGreen® Dead reagent were added to each well of cells. The cells were incubated at 37°C with 5% CO_2 for 10 minutes then imaged using a Leica SPEII confocal microscope.

Real-time reverse transcription-polymerase chain reaction. Total RNA was extracted from cultured cells using the isolate II RNA mini kit (Meridian Bioscence, Memphis, Tennessee, USA). cDNA was amplified and quantified using the SensiFast no-ROX SYBR-Green master mix on a micPCR machine. Primers for mms6 were used with housekeeping gene, glyceraldehyde 3-phosphate dehydrogenase (GAPDH), for normalization control. The relative amount of mRNA compared with GAPDH level was calculated using crossing point (Cp) values. Results of gene expression were plotted compared to control.

5.3 Results

Confirmation of mms6 gene expression and R2 signal in PANC-mms6 cells

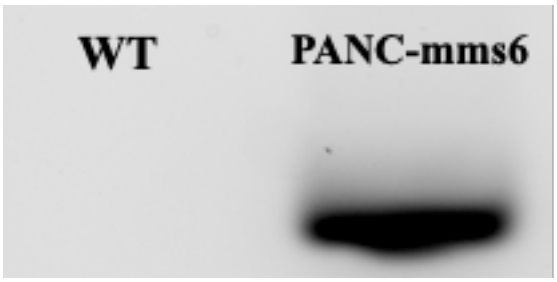

Figure 7: RT-PCR of mms6 expression in PANC-WT and PANC-mms6 cells

In Figure 7, we used RT-PCR to measure relative expression of the *mms6* gene in PANC-mms6 cells compared to WT control. Once gene expression was confirmed, PANC-mms6 and PANC-WT cells were fed 0, 100, and 200 μM of iron for 48 hours and R2/T2 relaxation was measured using a 3T Siemens MR scanner. The average R2 values of WT control cells at concentrations 0, 100, and 200 μM were 4.03, 2.93, and 4.37, respectively. In PANC-mms6 cells, we observed an increase in R2 signal (3.29, 5.28, 5.84) dependent on iron concentration. Iron buffer controls also showed minimal increase (1.47, 1.43, 1.75). We see a significant increase in signal for PANC-mms6 cells compared to WT when supplemented with 100 μM iron ($p = 1.77E-14$) and 200 μM iron ($p = 2.41E-14$). From these results, we propose the mms6 gene as a viable reporter for producing significant R2 signal in PANC-1 cells when compared to wild-type control PANC-1 cells.

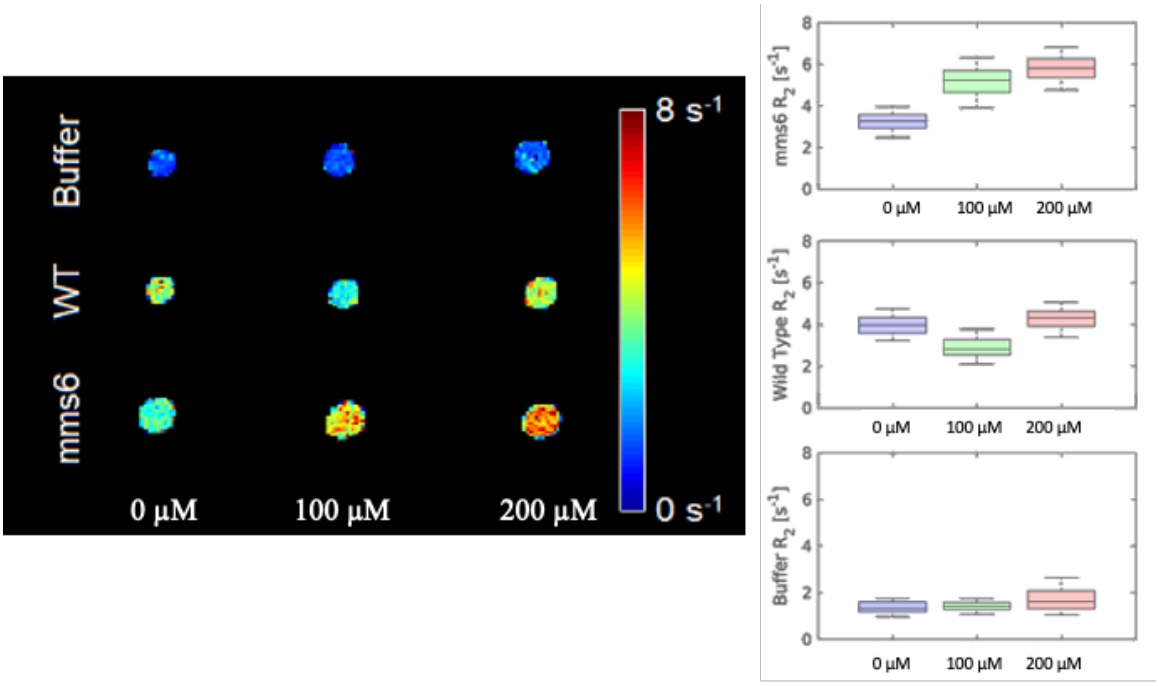

Figure 8: R2 signal produced from T2-weighted MRI scan.

Antiproliferative activity of pancreatic cancer cells in the presence of GEM and iron

In the current study, we tested the antiproliferative effect of gemcitabine and iron on PANC-1 (WT) and PANC-mms6 (mms6) cells *in vitro*. Cells were cultured in media supplemented with 0, 10 or 50 µM iron and 0, 20, 50, or 100 µM gemcitabine for 48 hours. The average proliferation rate of the WT cells ranged between 79.97 and 106.35% of the control rate. In the mms6 cell line, we observed a 81.1-86.7% reduction after treatment with both iron and gemcitabine despite varying concentrations. In the presence of only gemcitabine (20, 50, and 100 µM), mms6 cells showed a similar trend to cells

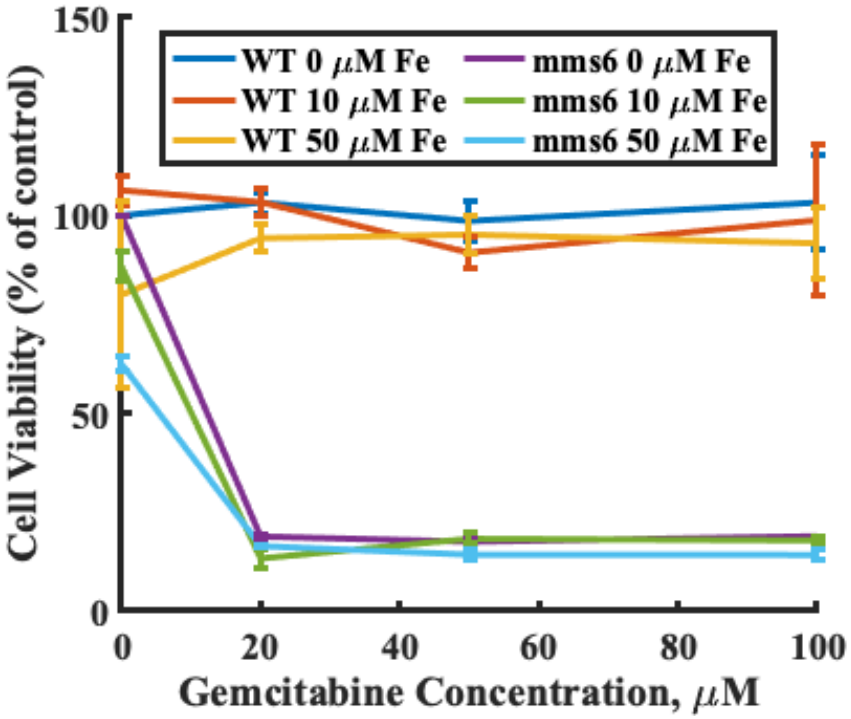

Figure 9: Antiproliferative activity of PANC-mms6 cells vs PANC-WT after treatment with GEM and iron. Cells were incubated for 48 hours in varying concentrations of GEM (0, 20, 50, and 100 μM) and iron (0, 10, 50 μM). N = 3 for each treatment group. All measurements were normalized to the untreated control for each cell line.

treated with both GEM and iron (81.09-82.45%). In mms6 cells treated exclusively with 10 and 50 μM iron, the proliferation rate was reduced by 13 and 38%, respectively. Chi-squared tests were performed comparing PANC-mms6 cells to the WT cells in 0, 10, and 50 Fe treatment groups (p-values: $4.468*10^{-44}$, $2.148*10^{-44}$, and $7.165*10^{-44}$, respectively). These results suggest that gemcitabine and iron inhibit mms6 cell proliferation at a greater rate than in WT cells. To confirm cell death, a live/dead assay was performed on WT and PANC-mms6 cells after 24- and 48-hour treatment with 50 μM GEM and 50 μM iron (Figure 10).

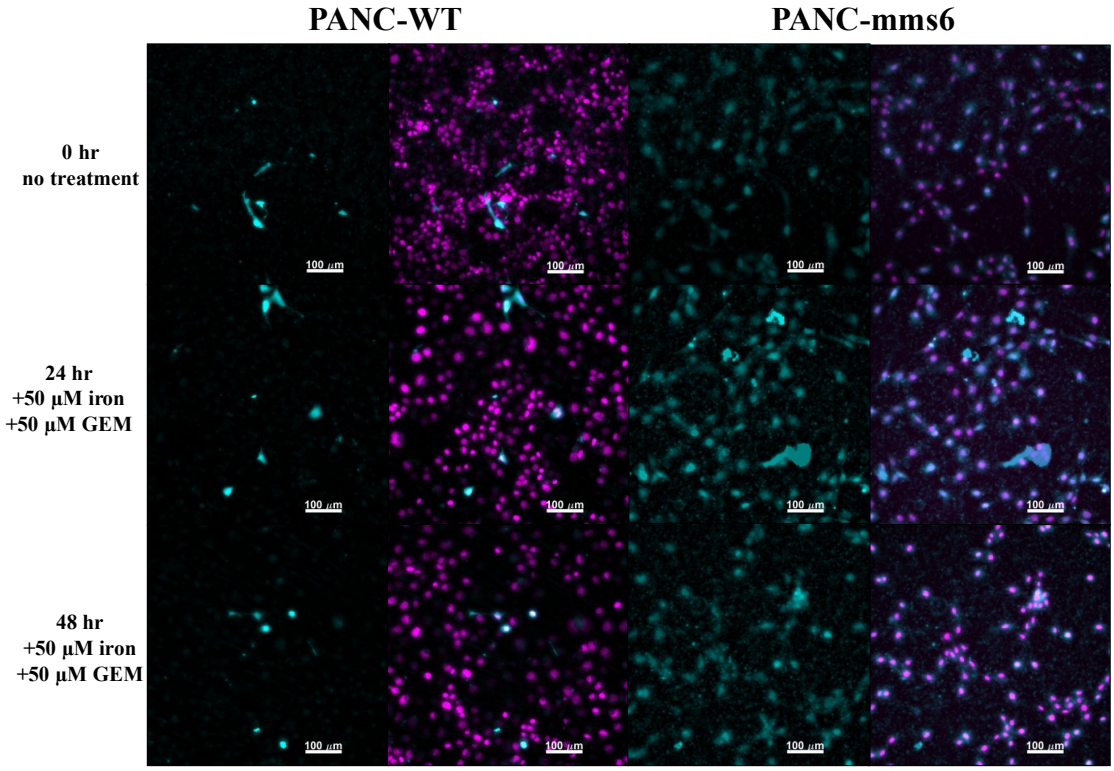

Figure 10: Live/dead assay qualitatively compares cell death in PANC-mms6 cells vs PANC-WT after 0-, 24-, and 48-hour treatment with 50 µM GEM and 50 µM iron. All cell nuclei are stained with Hoechst and shown in magenta. Dead cells are shown in cyan. Scale bar = 100 µm.

Nuclei of all cells were stained with Hoescht and shown in magenta. Dead cells were stained with NucGreen and shown in cyan. Despite the higher cell count, we observed less dead WT cells across all treatment time points. These data correlate with the viability data observed for both cell lines.

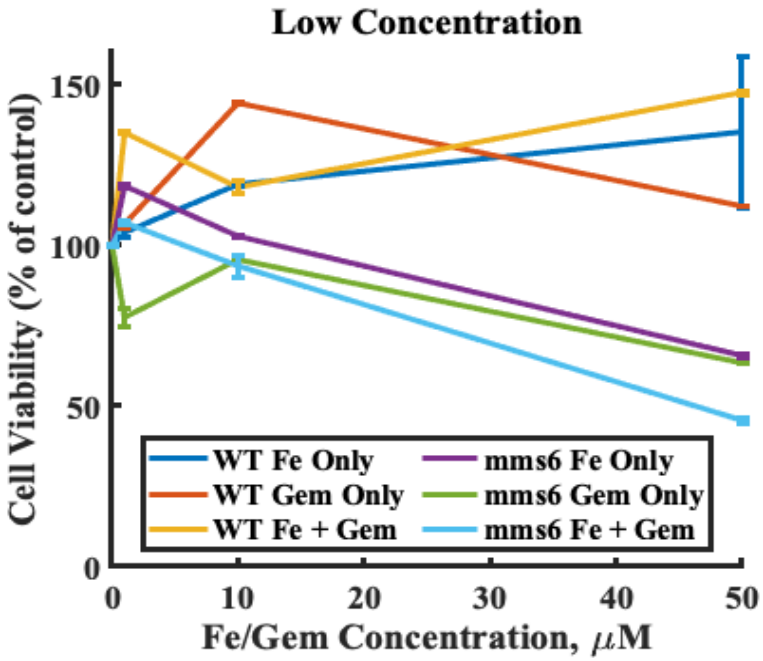

Figure 11: Antiproliferative activity of PANC-mms6 cells vs PANC-WT after treatment with lower doses of GEM and iron. Cells were incubated for 48 hours in varying concentrations of GEM (0, 1, 10, and 50 μM) and iron (0, 10, 50 μM). N = 3 for

Cell viability and IC50 values with lower concentration of GEM and iron

We then observed antiproliferative effect on WT and mms6 cells at lower concentrations of GEM and iron for 24 hours. For cell treated with only gemcitabine, the IC50 value was calculated to be 76.53 μM. Chi-squared analysis of cell viability showed significant difference with a p-value of 7.088E-10 between wild-type (expected) and mms6 (observed) cells. For iron only treatment, the IC50 value was 57.85 μM and a chi-squared p-value of 1.074E-08 between wild-type and mms6 cells. For combination treatment of GEM and iron, we calculated 43.4 μM and a chi-squared p-value of 1.544E-17 between wild-type and mms6 cells.

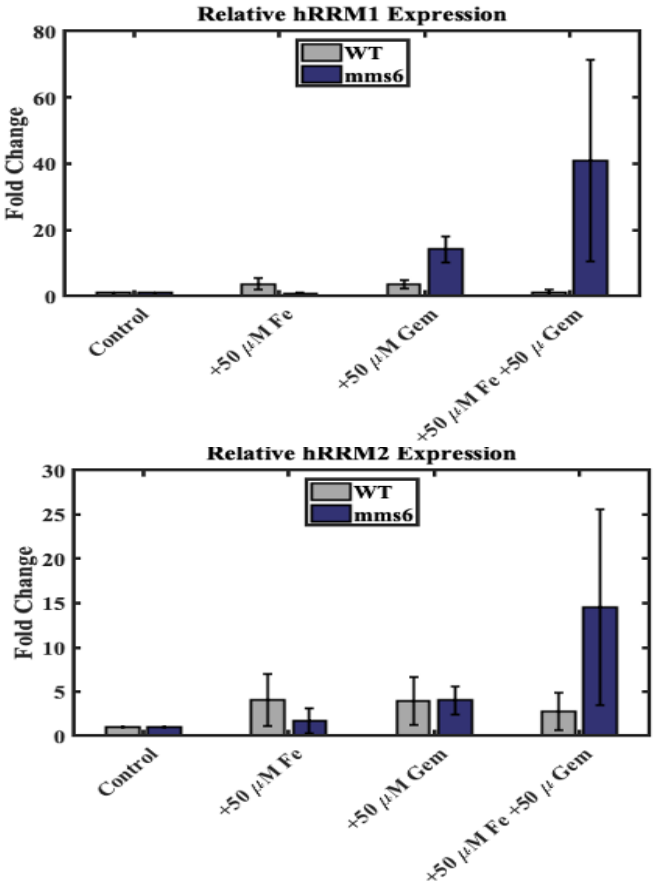

Figure 12: Relative gene expression of hRRM1 with and without iron and GEM treatment. hRRM1 expression in WT and PANC-mms6 cells after 48-hour incubation in 50 μM iron and/or GEM.

Expression of human ribonucleotide reductase subunits 1 and 2 (hRRM1/hRRM2)

To investigate a mechanism for cell viability disruption, we used quantitative RT-PCR data to measure expression of human RRM1 and RRM2 in PANC-WT and PANC-mms6 cells. Expression in both cell lines was observed 48 hours post treatment with 50 μM GEM, 50 μM iron, and 50 μM GEM/50 μM iron. Relative expression was quantified and normalized using GAPDH housekeeping gene. hRRM1 expression was low (<3.74 fold) across all treatments in WT cells. In GEM only and iron + GEM PANC-mms6 cells, hRRM1 increases (not significant; p = 04134). For hRRM2 expression, we see a similar consistent trend in WT cells (<4.1 fold). In PANC-mms6 cells, GEM only cells were similar to WT in expression. Iron + GEM treated cells

showed 14.55-fold change compared to 2.74 fold in WTs showing an increase in hRRM2 as well (not significant, $p = 0.4348$).

5.4 Discussion

In recent years, genes from magnetotactic bacteria have been utilized as MRI reporter genes; many are found in the magnetosome island within the genome. The *mms6* gene has mostly been investigated for its potential to produce local endogenous contrast agent in tumor cells (Elfick et al., 2017; Nudelman et al., 2018; Zhang et al., 2014). The role of mms6 in magnetotactic bacteria is to control magnetite crystallization for magnetosome production. Even when the gene is inserted into mammalian cells, it exhibits strong iron binding activity and allows for increased uptake and packaging in the cytoplasm (Nudelman et al., 2018). There are currently no studies investigating the effect of chemotherapy drugs on cancer cell lines engineered with mms6 or any other magnetotactic genes. For this study, we virally transduced *mms6* into PANC-1 cells and evaluated cell viability after treatment with iron (ferric citrate) and gemcitabine (GEM).

Although GEM is the key drug for treating pancreatic cancer, gemcitabine resistance remains a constant issue (Khan et al., 2019; Shinoda et al., 2018). In Figure 2A, we have demonstrated that PANC-mms6 cells experience a reduction in viability after treatment with GEM and iron. PANC-1 WT cells show stable viability (>86%) across multiple concentrations of both GEM (0, 20, 50, and 100 μM) and iron (0, 10, and 50 μM). In figure 2B, cell death was qualitatively evaluated by live/dead assay. The PANC-mms6 cells showed significantly more cell death in response treatment compared to the PANC-

WT cells. Our findings indicate that the mms6 gene allows for decreased GEM resistance in PANC-1 cells and has the potential to enhance gemcitabine therapy in pancreatic tumors.

Next, we investigated the role of ribonucleotide reductase (RR) subunit expression in response to GEM/iron treatment in PANC-mms6 and PANC-WT cells. RR is responsible for converting ribonucleotides to deoxyribonucleotides, which are essential for DNA polymerization and repair as well as maintaining the deoxynucleotide (dNTP) pool (Shinoda et al., 2018). RR catalytic activity relies on expression of subunits RRM1 and RRM2, where RRM2 requires iron for stabilization. Without iron supplementation to RRM2, RRM1 will become inactivated. The major difference between the PANC-mms6 and PANC-WT cells is the former's ability to accumulate more iron. Therefore, we decided to evaluate RRM1 and RRM2 expression levels in both cell lines after treatment with GEM and/or iron (Figure 3). We observed a significant increase in expression of both RRM1 and RRM2 in PANC-mms6 cells following 48-hour treatment with 50 μM GEM and 50 μM iron. In similar studies, increased expression of both subunits is associated with gemcitabine resistance, but our PANC-mms6 cell line produced the opposite effect. A possible mechanism might be: an increase in dNTP production and additional iron accumulation overloads the cell with free radicals leading to death.

In conclusion, we have developed a magnetic cancer cell line, PANC-mms6, and demonstrated the ability to enhance gemcitabine toxicity in pancreatic cancer cells engineered with bacterial gene, *mms6.* We have also noted an increase in expression of

ribonucleotide reductase subunits: hRRM1 and hRRM2. In future studies, *in vivo* tumor targeted treatment and further molecular analysis of the cell death mechanism will provide more detail on using the *mms6* gene with gemcitabine therapy as a possible treatment for pancreatic cancer.

CHAPTER SIX

CONCLUSIONS

The projects described in this dissertation are inspired by the therapeutic potential of MRI reporters. Creatine was first studied in this lab as a possible therapeutic technique for improving brain functions like cognition or memory. We set up a series of experiments where we developed a creatine nasal spray and tested whether we could get a significant increase in creatine concentration in mouse brain. For each round of experiments, six mice were used per treatment group (creatine treatment and nontreatment control). First, we administered 2.5 mg of creatine HCl and immediately measured creatine concentration in the dissected brain tissue 1 hour post administration. Results revealed no indication of an increase in brain creatine levels. We repeated the experiment four times and increase amount of creatine administered (2.5, 5, and 7 mg total per day) and duration of administration period (1 day, 5 days, 4 weeks). After sacrificing the mice, we measured creatine and creatinine concentration by a colorimetric enzymatic assay. Unfortunately, we did not collect any significant data that indicated an increase in brain creatine from the nasal spray experiments. Perhaps this study is better suited for humans, whom can be instructed to insufflate and actively take up more creatine through the nasal passage as opposed to the esophagus. Future studies on subjects with more brain volume will also allow for proper MRI contrast with better resolution. Nevertheless, while troubleshooting

the main project, we developed a method for measuring total creatine by converting all creatine species to creatinine and measuring its resulting concentration. With this method, it is possible to calculate each creatine metabolite. By combining creatine and creatinine biochemical assays with this technique, phosphocreatine concentration can be calculated from the raw measurements of Cr, Crn, and total Cr. This method was demonstrated on creatine and phosphocreatine standards as well as mouse skeletal muscle and brain tissue.

In the second project inspired by MRI reporters, we demonstrated the therapeutic effect of gemcitabine on pancreatic cancer cells engineered with iron-binding gene, *mms6*. The mms6 gene was isolated from magnetotactic bacteria and found to be a key gene in regulating magnetite crystal growth and morphology. When inserted into mammalian cells, they were able to take up and store more iron. More iron taken up by the cells provides better negative contrast for T2 and T2*-weighted imaging, making *mms6* a potential MR reporter gene for cell tracking. After stable expression of *mms6* was established in PANC-1 cells, we treated the cells with GEM and iron for 48 hours. Reduction in cell viability was pronounced in PANC-mms6 line compared to the wild-type. Cell proliferation and death were confirmed by MTT and live/dead assays. Expression of ribonucleotide reductase M1 and M2 were significantly increased in PANC-mms6 after 48-hour treatment with 50 μM GEM and 50 μM iron. Further studies include taking a better look at cellular death mechanism and the possible role of

reactive oxygen species, in vivo studies with tumor targeting, and gemcitabine treatment while relying on only endogenous iron.

BIBLIOGRAPHY

Akhavan, J. (2011). *The Chemistry of Explosives*. Royal Society of Chemistry.

Allen, P. J. (2012). Creatine metabolism and psychiatric disorders: Does creatine supplementation have therapeutic value? *Neuroscience and Biobehavioral Reviews*, *36*(5), 1442–1462. https://doi.org/10.1016/j.neubiorev.2012.03.005

Amano, S., Kaino, S., Shinoda, S., Harima, H., Matsumoto, T., Fujisawa, K., Takami, T., Yamamoto, N., Yamasaki, T., & Sakaida, I. (2020). Invasion inhibition in pancreatic cancer using the oral iron chelating agent deferasirox. *BMC Cancer*, *20*(1), 681. https://doi.org/10.1186/s12885-020-07167-8

Avgerinos, K. I., Spyrou, N., Bougioukas, K. I., & Kapogiannis, D. (2018). Effects of creatine supplementation on cognitive function of healthy individuals: A systematic review of randomized controlled trials. *Experimental Gerontology*, *108*, 166–173. https://doi.org/10.1016/j.exger.2018.04.013

Beard, H. H. (1941). The Biochemistry of Creatine and Creatinine. *Annual Review of Biochemistry*, *10*(1), 245–264. https://doi.org/10.1146/annurev.bi.10.070141.001333

Bird, S. P. (2003). Creatine Supplementation and Exercise Performance: A Brief Review. *Journal of Sports Science & Medicine*, *2*(4), 123–132.

Blakemore, R. (1975). Magnetotactic bacteria. *Science*, *190*(4212), 377–379. https://doi.org/10.1126/science.170679

Borsook: The hydrolysis of phosphocreatine and the... - Google Scholar. (n.d.). Retrieved July 15, 2021, from https://scholar.google.com/scholar_lookup?title=The%20hydrolysis%20of%20phosphocreatine%20and%20the%20origin%20of%20urinary%20creatinine&journal=J%20Biol%20Chem&volume=168&pages=493-510&publication_year=1947&author=Borsook%2CH&author=Dubnoff%2CJW

Brosnan, J. T., & Brosnan, M. E. (2007). Creatine: Endogenous metabolite, dietary, and therapeutic supplement. *Annual Review of Nutrition*, *27*, 241–261. https://doi.org/10.1146/annurev.nutr.27.061406.093621

Brosnan, M. E., & Brosnan, J. T. (2016). The role of dietary creatine. *Amino Acids*, *48*(8), 1785–1791. https://doi.org/10.1007/s00726-016-2188-1

Chanutin, A. (1927). A study of the effect of creatine on growth and its distribution in the tissues of normal rats. *Journal of Biological Chemistry*, *75*(2), 549–557.

Clark, J. F. (1997). Creatine and Phosphocreatine: A Review of Their Use in Exercise and Sport. *Journal of Athletic Training*, *32*(1), 45–51.

Elfick, A., Rischitor, G., Mouras, R., Azfer, A., Lungaro, L., Uhlarz, M., Herrmannsdörfer, T., Lucocq, J., Gamal, W., Bagnaninchi, P., Semple, S., & Salter, D. M. (2017). Biosynthesis of magnetic nanoparticles by human mesenchymal stem cells following transfection with the magnetotactic bacterial gene mms6. *Scientific Reports*, *7*(1), 39755. https://doi.org/10.1038/srep39755

Gilad, A. A., Winnard Jr, P. T., van Zijl, P. C., & Bulte, J. W. (2007). Developing MR reporter genes: Promises and pitfalls. *NMR in Biomedicine: An International Journal Devoted to the Development and Application of Magnetic Resonance In Vivo*, *20*(3), 275–290.

Gilad, A. A., Ziv, K., McMahon, M. T., Zijl, P. C. M. van, Neeman, M., & Bulte, J. W. M. (2008). MRI Reporter Genes. *Journal of Nuclear Medicine*, *49*(12), 1905–1908. https://doi.org/10.2967/jnumed.108.053520

Guo, R., Zhang, M., Xi, Y., Ma, Y., Liang, S., Shi, S., Miao, Y., & Li, B. (2014). Theranostic Studies of Human Sodium Iodide Symporter Imaging and Therapy Using 188Re: A Human Glioma Study in Mice. *PLoS ONE*, *9*(7). https://doi.org/10.1371/journal.pone.0102011

Haris, M., Nanga, R. P. R., Singh, A., Cai, K., Kogan, F., Hariharan, H., & Reddy, R. (2012). Exchange Rates of Creatine Kinase Metabolites: Feasibility of Imaging Creatine by Chemical Exchange Saturation Transfer MRI. *NMR in Biomedicine*, *25*(11). https://doi.org/10.1002/nbm.2792

Harris, R., Söderlund, K., & Hultman, E. (1992). Elevation of creatine in resting and exercised muscle of normal subjects by creatine supplementation. *Clinical Science*. https://doi.org/10.1042/CS0830367

Hentze, M. W., Muckenthaler, M. U., & Andrews, N. C. (2004). Balancing acts: Molecular control of mammalian iron metabolism. *Cell*, *117*(3), 285–297. https://doi.org/10.1016/s0092-8674(04)00343-5

Ishimaru, H., Morikawa, M., Iwanaga, S., Kaminogo, M., Ochi, M., & Hayashi, K. (2001). Differentiation between high-grade glioma and metastatic brain tumor using single-voxel proton MR spectroscopy. *European Radiology*, *11*(9), 1784–1791. https://doi.org/10.1007/s003300000814

Jabs, C. M., Nëglen, P., Eklöf, B., & Thomas, E. J. (1988). Plasma creatine determination using a luminescence method. *Biochemical Medicine and Metabolic Biology*, *39*(3), 267–272. https://doi.org/10.1016/0885-4505(88)90084-9

Jaffe, M. (1886). Ueber den Niederschlag, welchen Pikrinsäure in normalem Harn erzeugt und über eine neue Reaction des Kreatinins. *Biological Chemistry*, *10*(5), 391–400. https://doi.org/10.1515/bchm1.1886.10.5.391

Khan, S., Setua, S., Kumari, S., Dan, N., Massey, A., Hafeez, B. B., Yallapu, M. M., Stiles, Z. E., Alabkaa, A., Yue, J., Ganju, A., Behrman, S., Jaggi, M., & Chauhan, S. C. (2019). Superparamagnetic iron oxide nanoparticles of curcumin enhance gemcitabine therapeutic response in pancreatic cancer. *Biomaterials*, *208*, 83–97. https://doi.org/10.1016/j.biomaterials.2019.04.005

Kharkar, P. B., Talkar, S. S., Kadwadkar, N. A., & Patravale, V. B. (2017). Chapter 11—Nanosystems for oral delivery of immunomodulators. In E. Andronescu & A. M. Grumezescu (Eds.), *Nanostructures for Oral Medicine* (pp. 295–334). Elsevier. https://doi.org/10.1016/B978-0-323-47720-8.00012-2

Kush, P., Bajaj, T., Kaur, M., Madan, J., Jain, U. K., Kumar, P., Deep, A., & Kim, K.-H. (2020). Biodistribution and Pharmacokinetic Study of Gemcitabine Hydrochloride Loaded Biocompatible Iron-Based Metal Organic Framework. *Journal of Inorganic and Organometallic Polymers and Materials*, *30*(8), 2827–2841. https://doi.org/10.1007/s10904-019-01417-4

Ladd, M. E., Bachert, P., Meyerspeer, M., Moser, E., Nagel, A. M., Norris, D. G., Schmitter, S., Speck, O., Straub, S., & Zaiss, M. (2018). Pros and cons of ultra-high-field MRI/MRS for human application. *Progress in Nuclear Magnetic Resonance Spectroscopy*, *109*, 1–50. https://doi.org/10.1016/j.pnmrs.2018.06.001

Li, Z., Qiao, H., Lebherz, C., Choi, S. R., Zhou, X., Gao, G., Kung, H. F., Rader, D. J., Wilson, J. M., Glickson, J. D., & Zhou, R. (2005). Creatine kinase, a magnetic resonance-detectable marker gene for quantification of liver-directed gene transfer. *Human Gene Therapy*, *16*(12), 1429–1438. https://doi.org/10.1089/hum.2005.16.1429

Matthews, R. T., Ferrante, R. J., Klivenyi, P., Yang, L., Klein, A. M., Mueller, G., Kaddurah-Daouk, R., & Beal, M. F. (1999). Creatine and cyclocreatine attenuate MPTP neurotoxicity. *Experimental Neurology*, *157*(1), 142–149. https://doi.org/10.1006/exnr.1999.7049

McGuigan, A., Kelly, P., Turkington, R. C., Jones, C., Coleman, H. G., & McCain, R. S. (2018). Pancreatic cancer: A review of clinical diagnosis, epidemiology, treatment

and outcomes. *World Journal of Gastroenterology*, *24*(43), 4846–4861. https://doi.org/10.3748/wjg.v24.i43.4846

McKenna, M. J., Morton, J., Selig, S. E., & Snow, R. J. (1999). Creatine supplementation increases muscle total creatine but not maximal intermittent exercise performance. *Journal of Applied Physiology*, *87*(6), 2244–2252. https://doi.org/10.1152/jappl.1999.87.6.2244

Meister, A. (2009). *Advances in Enzymology and Related Areas of Molecular Biology*. John Wiley & Sons.

Menon, R. G., Xia, D., Katz, S. D., & Regatte, R. R. (2021). Dynamic 31P-MRI and 31P-MRS of lower leg muscles in heart failure patients. *Scientific Reports*, *11*. https://doi.org/10.1038/s41598-021-86392-y

Mercimek-Andrews, S., & Salomons, G. S. (1993). Creatine Deficiency Syndromes. In M. P. Adam, H. H. Ardinger, R. A. Pagon, S. E. Wallace, L. J. Bean, G. Mirzaa, & A. Amemiya (Eds.), *GeneReviews®*. University of Washington, Seattle. http://www.ncbi.nlm.nih.gov/books/NBK3794/

Miller, B. F., Allinson, M. C., & Baker, Z. (1939). STUDIES ON THE METABOLISM OF CREATINE AND CREATININE I. SPECIFIC ENZYMATIC METHODS FOR THE ANALYSIS OF CREATINE AND CREATININE IN TISSUES. *Journal of Biological Chemistry*, *130*(1), 383–391.

Murat, D., Quinlan, A., Vali, H., & Komeili, A. (2010). Comprehensive genetic dissection of the magnetosome gene island reveals the step-wise assembly of a prokaryotic organelle. *Proceedings of the National Academy of Sciences*, *107*(12), 5593–5598.

Nudelman, H., Lee, Y.-Z., Hung, Y.-L., Kolusheva, S., Upcher, A., Chen, Y.-C., Chen, J.-Y., Sue, S.-C., & Zarivach, R. (2018). Understanding the Biomineralization Role of Magnetite-Interacting Components (MICs) From Magnetotactic Bacteria. *Frontiers in Microbiology*, *9*. https://doi.org/10.3389/fmicb.2018.02480

Pan, J. W., & Takahashi, K. (2007). Cerebral energetic effects of creatine supplementation in humans. *American Journal of Physiology. Regulatory, Integrative and Comparative Physiology*, *292*(4), R1745–R1750. https://doi.org/10.1152/ajpregu.00717.2006

Peake, *Michael, & Whiting, M. (2006). Measurement of Serum Creatinine – Current Status and Future Goals. *Clinical Biochemist Reviews*, *27*(4), 173–184.

Penet, M.-F., Jin, J., Chen, Z., & Bhujwalla, Z. M. (2016). Magnetic Resonance Imaging and Spectroscopy in Cancer Theranostic Imaging. *Topics in Magnetic Resonance Imaging : TMRI*, *25*(5), 215–221. https://doi.org/10.1097/RMR.0000000000000098

Persky, A. M., & Brazeau, G. A. (2001). Clinical Pharmacology of the Dietary Supplement Creatine Monohydrate. *Pharmacological Reviews*, *53*(2), 161–176.

Pruis, I. J., van Dongen, G. A. M. S., & Veldhuijzen van Zanten, S. E. M. (2020). The Added Value of Diagnostic and Theranostic PET Imaging for the Treatment of CNS Tumors. *International Journal of Molecular Sciences*, *21*(3). https://doi.org/10.3390/ijms21031029

Pulsipher, K. W., Hammer, D. A., Lee, D., & Sehgal, C. M. (2018). Engineering Theranostic Microbubbles Using Microfluidics for Ultrasound Imaging and Therapy: A Review. *Ultrasound in Medicine & Biology*, *44*(12), 2441–2460. https://doi.org/10.1016/j.ultrasmedbio.2018.07.026

Qiao, Z., He, M., He, M. U., Li, W., Wang, X., Wang, Y., Kuai, Q., Li, C., Ren, S., & Yu, Q. (2016). Synergistic antitumor activity of gemcitabine combined with triptolide in pancreatic cancer cells. *Oncology Letters*, *11*(5), 3527–3533. https://doi.org/10.3892/ol.2016.4379

Richter, M., Kube, M., Bazylinski, D. A., Lombardot, T., Glöckner, F. O., Reinhardt, R., & Schüler, D. (2007). Comparative Genome Analysis of Four Magnetotactic Bacteria Reveals a Complex Set of Group-Specific Genes Implicated in Magnetosome Biomineralization and Function. *Journal of Bacteriology*, *189*(13), 4899–4910. https://doi.org/10.1128/JB.00119-07

Rose, W. C., Helmer, O. M., & Chanutin, A. (1927). A modified method for the estimation of total creatinine in small amounts of tissues. *Journal of Biological Chemistry*, *75*(2), 543–548.

Sellevold, O. F. M., Jynge, P., & Aarstad, K. (1986). High performance liquid chromatography: A rapid isocratic method for determination of creatine compounds and adenine nucleotides in myocardial tissue. *Journal of Molecular and Cellular Cardiology*, *18*(5), 517–527. https://doi.org/10.1016/S0022-2828(86)80917-8

Sherman, H. G., Jovanovic, C., Stolnik, S., Baronian, K., Downard, A. J., & Rawson, F. J. (2018). New Perspectives on Iron Uptake in Eukaryotes. *Frontiers in Molecular Biosciences*, *5*. https://doi.org/10.3389/fmolb.2018.00097

Shinoda, S., Kaino, S., Amano, S., Harima, H., Matsumoto, T., Fujisawa, K., Takami, T., Yamamoto, N., Yamasaki, T., & Sakaida, I. (2018). Deferasirox, an oral iron chelator, with gemcitabine synergistically inhibits pancreatic cancer cell growth in vitro and in vivo. *Oncotarget*, *9*(47), 28434–28444. https://doi.org/10.18632/oncotarget.25421

Stout, J. R., Eckerson, J. M., May, E., Coulter, C., & Bradley-Popovich, G. E. (2001). Effects of resistance exercise and creatine supplementation on myasthenia gravis: A case study. *Medicine & Science in Sports & Exercise*, *33*(6), 869–872.

Sun, N., Li, Q., Zhao, L., He, H., Zhang, M., & Wang, X. (2019). Simultaneous quantitative analysis of phosphocreatine, creatine and creatinine in plasma of children by HPLC–MS/MS method: Application to a pharmacokinetic study in children with viral myocarditis. *Biomedical Chromatography*, *33*(8), e4558. https://doi.org/10.1002/bmc.4558

Turner, C. E., & Gant, N. (2014). The biochemistry of creatine. In *Magnetic resonance spectroscopy* (pp. 91–103). Elsevier.

VANAKOSKIl, J., KOSUNENl, V., MERlRlNNEl, E., & SEPPÄLÄl, T. (n.d.). *Creatine and caffeine in anaerobic and aerobic exercise: Effects on physical performance and pharmacokinetic considerations*. 6.

Vandenberghe, K., Goris, M., Van Hecke, P., Van Leemputte, M., Vangerven, L., & Hespel, P. (1997). Long-term creatine intake is beneficial to muscle performance during resistance training. *Journal of Applied Physiology*, *83*(6), 2055–2063. https://doi.org/10.1152/jappl.1997.83.6.2055

Xiao, Y.-D., Paudel, R., Liu, J., Ma, C., Zhang, Z.-S., & Zhou, S.-K. (2016). MRI contrast agents: Classification and application (Review). *International Journal of Molecular Medicine*, *38*(5), 1319–1326. https://doi.org/10.3892/ijmm.2016.2744

Zhang, X.-Y., Robledo, B. N., Harris, S. S., & Hu, X. P. (2014). A bacterial gene, mms6, as a new reporter gene for magnetic resonance imaging of mammalian cells. *Molecular Imaging*, *13*. https://doi.org/10.2310/7290.2014.00046

Zurkiya, O., Chan, A. W. S., & Hu, X. (2008). MagA Is Sufficient for Producing Magnetic Nanoparticles in Mammalian Cells, Making it an MRI Reporter. *Magnetic Resonance in Medicine : Official Journal of the Society of Magnetic Resonance in Medicine / Society of Magnetic Resonance in Medicine*, *59*(6), 1225–1231. https://doi.org/10.1002/mrm.21606

APPENDIX

A. Full Transcript of pTwist-mms6 plasmid (optimized mms6 gene shown in bold text)

GCCGCCGCAATGGGAGAAATGGAAAGGGAAGGTGCAGCAGCAAAAGCT

GGCGCAGCGAAAACTGGAGCTGCAAAGACTGGTACAGTGGCAAAGACT

GGTATAGCTGCGAAAACCGGGGTCGCAACAGCGGTGGCTGCACCTGCC

GCACCAGCTAACGTGGCAGCAGCTCAAGGGGCTGGTACAAAAGTAGCAC

TGGGAGCTGGGAAAGCGGCGGCAGGAGCGAAAGTGGTTGGCGGCACTA

TTTGGACAGGCAAAGGTCTCGGTCTGGGACTTGGGTTGGGCTTGGGAGC

CTGGGGCCCCATTATCCTGGGAGTGGTCGGAGCTGGAGCCGTGTATGCC

TACATGAAATCACGCGACATTGAGAGTGCTCAATCCGATGAAGAGGTGG

AGTTGCGGGATGCCCTCGCTTAAACTAGTGTCTCGAGCTTATTCCAGATGC

GTGCGGATGGAATTCGAGCTCGGTACCATGCCAAAAGCAAAGCGCTATCGCG

CCTTACGTTACTGGCCGAAGCCGCTTGGAATAAGGCCGGTGTGCGTTTGTCTA

TATGTTATTTTCCACCATATTGCCGTCTTTTGGCAATGTGAGGGCCCGGAAAC

CTGGCCCTGTCTTCTTGACGAGCATTCCTAGGGGTCTTTCCCCTCTCGCCAAA

GGAATGCAAGGTCTGTTGAATGTCGTGAAGGAAGCAGTTCCTCTGGAAGCTT

CTTGAAGACAAACAACGTCTGTAGCGACCCTTTGCAGGCAGCGGAACCCCCC

ACCTGGCGACAGGTGCCTCTGCGGCCAAAAGCCACGTGTATAAGATACACCT

GCAAAGGCGGCACAACCCCAGTGCCACGTTGTGAGTTGGATAGTTGTGGAAA

GAGTCAAATGGCTCCCCTCAAGCGTATTCAACAAGGGGCTGAAGGATGCCCA

GAAGGTACCCCATTGTATGGGATCTGATCTGGGGCCTCGGTGCACATGCTTTT

CATGTGTTTAGTCGAGGTTAAAAAACGTCTAGGCCCCCCGAACCACGGGGAC

GTGGTTTTCCTTTGAAAAACACGATGATAATAACATGACCGAGTACAAGCCC

ACGGTGCGCCTCGCCACCCGCGACGACGTCCCCAGGGCCGTACGCACCCTCG

CCGCCGCGTTCGCCGACTACCCCGCCACGCGCCACACCGTCGATCCGGACCG

CCACATCGAGCGGGTCACCGAGCTGCAAGAACTCTTCCTCACGCGCGTCGGG

CTCGACATCGGCAAGGTGTGGGTCGCGGACGACGGCGCCGCGGTGGCGGTCT

GGACCACGCCGGAGAGCGTCGAAGCGGGGGCGGTGTTCGCCGAGATCGGCC

CGCGCATGGCCGAGTTGAGCGGTTCCCGGCTGGCCGCGCAGCAACAGATGGA

GGGCCTCCTGGCGCCGCACCGGCCCAAGGAGCCCGCGTGGTTCCTGGCCACC

GTCGGCGTCTCGCCCGACCACCAGGGCAAGGGTCTGGGCAGCGCCGTCGTGC

TCCCCGGAGTGGAGGCCGCCGAGCGCGCCGGGGTGCCCGCCTTCCTGGAGAC

CTCCGCGCCCCGCAACCTCCCCTTCTACGAGCGGCTCGGCTTCACCGTCACCG

CCGACGTCGAGGTGCCCGAAGGACCGCGCACCTGGTGCATGACCCGCAAGCC

CGGTGCCTAGGCTAGCTTGACTGACTGAGTCGACAATCAACCTTTTGGATTAC

AAAATTTGTGAAAGATTGACTGGTATTCTTAACTATGTTGCTCCTTTTACGCT

ATGTGGATACGCTGCTTTAATGCCTTTGTATCATGCTATTGCTTCCCGTATGGC

TTTCATTTTCTCCTCCTTGTATAAATCCTGGTTGCTGTCTCTTTATGAGGAGTT

GTGGCCCGTTGTCAGGCAACGTGGCGTGGTGTGCACTGTGTTTGCTGACGCA

ACCCCCACTGGTTGGGGCATTGCCACCACCTGTCAGCTCCTTTCCGGGACTTT

CGCTTTCCCCCTCCCTATTGCCACGGCGGAACTCATCGCCGCCTGCCTTGCCC

GCTGCTGGACAGGGGCTCGGCTGTTGGGCACTGACAATTCCGTGGTGTTGTC

GGGGAAGCTGACGTCCTTTCCATGGCTGCTCGCCTGTGTTGCCACCTGGATTC

TGCGCGGGACGTCCTTCTGCTACGTCCCTTCGGCCCTCAATCCAGCGGACCTT

CCTTCCCGCGGCCTGCTGCCGGCTCTGCGGCCTCTTCCGCGTCTTCGCCTTCG

CCCTCAGACGAGTCGGATCTCCCTTTGGGCCGCCTCCCCGCCTGGAATTCGAG

CTCGGTACCTTTAAGACCAATGACTTACAAGGCAGCTGTAGATCTTAGCCACT

TTTTAAAAGAAAAGGGGGGACTGGAAGGGCTAATTCACTCCCAACGAAGAC

AAGATCTGCTTTTTGCTTGTACTGGGTCTCTCTGGTTAGACCAGATCTGAGCC

TGGGAGCTCTCTGGCTAACTAGGGAACCCACTGCTTAAGCCTCAATAAAGCT

TGCCTTGAGTGCTTCAAGTAGTGTGTGCCCGTCTGTTGTGTGACTCTGGTAAC

TAGAGATCCCTCAGACCCTTTTAGTCAGTGTGGAAAATCTCTAGCAGTCCTGG

CCAACGTGAGCACCGTGCTGACCTCCAAATATCGTTAAGCTGGAGCCTGGGA

GCCGGCCTGGCCCTCCGCCCCCCCCACCCCCGCAGCCCACCCCTGGTCTTTGA

ATAAAGTCTGAGTGAGTGGCCGACAGTGCCCGTGGAGTTCTCGTGACCTGAG

GTGCAGGGCCGGCGCTAGGGACACGTCCGTGCACGTGCCGAGGCCCCCTGTG

CAGCTGCAAGGGACAGGCCTAGCCCTGCAGGCCTAACTCCGCCCATCCCGCC

CCTAACTCCGCCCAGTTCCGCCCATTCTCCGCCTCATGGCTGACTAATTTTTTT

TATTTATGCAGAGGCCGAGGCCGCCTCGGCCTCTGAGCTATTCCAGAAGTAG

TGAGGACGCTTTTTTGGAGGCCGAGGCTTTTGCAAAGATCGAACAAGAGACA

GGACCTGCAGGTTAATTAAATTTAAATCATGTGAGCAAAAGGCCAGCAAAAG

GCCAGGAACCGTAAAAAGGCCGCGTTGCTGGCGTTTTTCCATAGGCTCCGCC

CCCCTGACGAGCATCACAAAAATCGACGCTCAAGTCAGAGGTGGCGAAACCC

GACAGGACTATAAAGATACCAGGCGTTTCCCCCTGGAAGCTCCCTCGTGCGC

TCTCCTGTTCCGACCCTGCCGCTTACCGGATACCTGTCCGCCTTTCTCCCTTCG

GGAAGCGTGGCGCTTTCTCATAGCTCACGCTGTAGGTATCTCAGTTCGGTGTA

GGTCGTTCGCTCCAAGCTGGGCTGTGTGCACGAACCCCCCGTTCAGCCCGAC

CGCTGCGCCTTATCCGGTAACTATCGTCTTGAGTCCAACCCGGTAAGACACG

ACTTATCGCCACTGGCAGCAGCCACTGGTAACAGGATTAGCAGAGCGAGGTA

TGTAGGCGGTGCTACAGAGTTCTTGAAGTGGTGGCCTAACTACGGCTACACT

AGAAGAACAGTATTTGGTATCTGCGCTCTGCTGAAGCCAGTTACCTTCGGAA

AAAGAGTTGGTAGCTCTTGATCCGGCAAACAAACCACCGCTGGTAGCGGTGG

TTTTTTTGTTTGCAAGCAGCAGATTACGCGCAGAAAAAAAGGATCTCAAGAA

GATCCTTTGATCTTTTCTACGGGGTCTGACGCTCAGTGGAACGAAAACTCACG

TTAAGGGATTTTGGTCATGAGATTATCAAAAAGGATCTTCACCTAGATCCTTT

TAAATTAAAAATGAAGTTTTAAATCAATCTAAAGTATATATGAGTAAACTTG

GTCTGACAGTTACCAATGCTTAATCAGTGAGGCACCTATCTCAGCGATCTGTC

TATTTCGTTCATCCATAGTTGCATTTAAATGGCCGGCCTGGCGCGCCGTTTAA

ACCTAGATATTGATAGTCTGATCGGTCAACGTATAATCGAGTCCTAGCTTTTG

CAAACATCTATCAAGAGACAGGATCAGCAGGAGGCTTTCGCATGAGTATTCA

ACATTTCCGTGTCGCCCTTATTCCCTTTTTTGCGGCATTTTGCCTTCCTGTTTTT

GCTCACCCAGAAACGCTGGTGAAAGTAAAAGATGCTGAAGATCAGTTGGGTG

CGCGAGTGGGTTACATCGAACTGGATCTCAACAGCGGTAAGATCCTTGAGAG

TTTTCGCCCCGAAGAACGCTTTCCAATGATGAGCACTTTTAAAGTTCTGCTAT

GTGGCGCGGTATTATCCCGTATTGACGCCGGGCAAGAGCAACTCGGTCGCCG

CATACACTATTCTCAGAATGACTTGGTTGAGTATTCACCAGTCACAGAAAAG

CATCTTACGGATGGCATGACAGTAAGAGAATTATGCAGTGCTGCCATAACCA

TGAGTGATAACACTGCGGCCAACTTACTTCTGACAACGATTGGAGGACCGAA

GGAGCTAACCGCTTTTTTGCACAACATGGGGGATCATGTAACTCGCCTTGATC

GTTGGGAACCGGAGCTGAATGAAGCCATACCAAACGACGAGCGTGACACCA

CGATGCCTGTAGCAATGGCAACAACCTTGCGTAAACTATTAACTGGCGAACT

ACTTACTCTAGCTTCCCGGCAACAGTTGATAGACTGGATGGAGGCGGATAAA

GTTGCAGGACCACTTCTGCGCTCGGCCCTTCCGGCTGGCTGGTTTATTGCTGA

TAAATCTGGAGCCGGTGAGCGTGGGTCTCGCGGTATCATTGCAGCACTGGGG

CCAGATGGTAAGCCCTCCCGTATCGTAGTTATCTACACGACGGGGAGTCAGG

CAACTATGGATGAACGAAATAGACAGATCGCTGAGATAGGTGCCTCACTGAT

TAAGCATTGGTAACCGATTCTAGGTGCATTGGCGCAGAAAAAAATGCCTGAT

GCGACGCTGCGCGTCTTATACTCCCACATATGCCAGATTCAGCAACGGATAC

GGCTTCCCCAACTTGCCCACTTCCATACGTGTCCTCCTTACCAGAAATTTATC

CTTAAGATCCCGAATCGTTTAAACGCGATCGCAGTAATCAATTACGGGGTCA

TTAGTTCATAGCCCATATATGGAGTTCCGCGTTACATAACTTACGGTAAATGG

CCCGCCTGGCTGACCGCCCAACGACCCCCGCCCATTGACGTCAATAATGACG

TATGTTCCCATAGTAACGCCAATAGGGACTTTCCATTGACGTCAATGGGTGGA

GTATTTACGGTAAACTGCCCACTTGGCAGTACATCAAGTGTATCATATGCCAA

GTACGCCCCCTATTGACGTCAATGACGGTAAATGGCCCGCCTGGCATTATGC

CCAGTACATGACCTTATGGGACTTTCCTACTTGGCAGTACATCTACGTATTAG

TCATCGCTATTACCATGGTGATGCGGTTTTGGCAGTACATCAATGGGCGTGGA

TAGCGGTTTGACTCACGGGGATTTCCAAGTCTCCACCCCATTGACGTCAATGG

GAGTTTGTTTTGGCACCAAAATCAACGGGACTTTCCAAAATGTCGTAACAACT

CCGCCCCATTGACGCAAATGGGCGGTAGGCGTGTACGGTGGGAGGTCTATAT

AAGCAGAGCTCGTTTAGTGAACCGGGGTCTCTCTGGTTAGACCAGATCTGAG

CCTGGGAGCTCTCTGGCTAACTAGGGAACCCACTGCTTAAGCCTCAATAAAG

CTTGCCTTGAGTGCTTCAAGTAGTGTGTGCCCGTCTGTTGTGTGACTCTGGTA

ACTAGAGATCCCTCAGACCCTTTTAGTCAGTGTGGAAAATCTCTAGCAGTGGC

GCCCGAACAGGGACCTGAAAGCGAAAGGGAAACCAGAGCTCTCTCGACGCA

GGACTCGGCTTGCTGAAGCGCGCACGGCAAGAGGCGAGGGGCGGCGACTGG

TGAGTACGCCAAAAATTTTGACTAGCGGAGGCTAGAAGGAGAGAGATGGGT

GCGAGAGCGTCAGTATTAAGCGGGGGAGAATTAGATCGCGATGGGAAAAAA

TTCGGTTAAGGCCAGGGGGAAAGAAAAAATATAAATTAAAACATATAGTATG

GGCAAGCAGGGAGCTAGAACGATTCGCAGTTAATCCTGGCCTGTTAGAAACA

TCAGAAGGCTGTAGACAAATACTGGGACAGCTACAACCATCCCTTCAGACAG

GATCAGAAGAACTTAGATCATTATATAATACAGTAGCAACCCTCTATTGTGTG

CATCAAAGGATAGAGATAAAAGACACCAAGGAAGCTTTAGACAAGATAGAG

GAAGAGCAAAACAAAAGTAAGACCACCGCACAGCAAGCGGCCGCTGATCTT

CAGACCTGGAGGAGGAGATATGAGGGACAATTGGAGAAGTGAATTATATAA

ATATAAAGTAGTAAAAATTGAACCATTAGGAGTAGCACCCACCAAGGCAAA

GAGAAGAGTGGTGCAGAGAGAAAAAAGAGCAGTGGGAATAGGAGCTTTGTT

CCTTGGGTTCTTGGGAGCAGCAGGAAGCACTATGGGCGCAGCCTCAATGACG

CTGACGGTACAGGCCAGACAATTATTGTCTGGTATAGTGCAGCAGCAGAACA

ATTTGCTGAGGGCTATTGAGGCGCAACAGCATCTGTTGCAACTCACAGTCTG

GGGCATCAAGCAGCTCCAGGCAAGAATCCTGGCTGTGGAAAGATACCTAAAG

GATCAACAGCTCCTGGGGATTTGGGGTTGCTCTGGAAAACTCATTTGCACCAC

TGCTGTGCCTTGGAATGCTAGTTGGAGTAATAAATCTCTGGAACAGATTTGGA

ATCACACGACCTGGATGGAGTGGGACAGAGAAATTAACAATTACACAAGCTT

AATACACTCCTTAATTGAAGAATCGCAAAACCAGCAAGAAAAGAATGAACA

AGAATTATTGGAATTAGATAAATGGGCAAGTTTGTGGAATTGGTTTAACATA

ACAAATTGGCTGTGGTATATAAAATTATTCATAATGATAGTAGGAGGCTTGG

TAGGTTTAAGAATAGTTTTTGCTGTACTTTCTATAGTGAATAGAGTTAGGCAG

GGATATTCACCATTATCGTTTCAGACCCACCTCCCAACCCCGAGGGGACCCG

ACAGGCCCGAAGGAATAGAAGAAGAAGGTGGAGAGAGAGACAGAGACAGA

TCCATTCGATTAGTGAACGGATCTCGACGGTATCGGTTAACTTTTAAAAGAAA

AGGGGGGATTGGGGGGTACAGTGCAGGGGAAAGAATAGTAGACATAATAGC

AACAGACATACAAACTAAAGAATTACAAAAACAAATTACAAAAATTCAAAA

TTTTGGCTCCCGATCGTTGCGTTACACACACAATTACTGCTGATCGAGTGTAG

CCTTCGAATGAAAGACCCCACCTGTAGGTTTGGCAAGATAGCTGCAGTAACG

CCATTTTGCAAGGCATGGAAAAATACCAAACCAAGAATAGAGAAGTTCAGAT

CAAGGGCGGGTACATGAAAATAGCTAACGTTGGGCCAAACAGGATATCTGCG

GTGAGCAGTTTCGGCCCCGGCCCGGGGCCAAGAACAGATGGTCACCGCAGTT

TCGGCCCCGGCCCGAGGCCAAGAACAGATGGTCCCCAGATATGGCCCAACCC

TCAGCAGTTTCTTAAGACCCATCAGATGTTTCCAGGCTCCCCCAAGGACCTGA

AATGACCCTGCGCCTTATTTGAATTAACCAATCAGCCTGCTTCTCGCTTCTGTT

CGCGCGCTTCTGCTTCCCGAGCTCTATAAAAGAGCTCACAACCCCTCACTCGG

CGCGCCAGTCCTCCGATTGACTGAGTCGCCCTGATCATTGTCGATCCTACCAT

CCACTCGACACACCCGCCAGGGCCCGCATCCACCATCGCAGACTTATCATGG

ATCCTGACGCGT

MATLAB code for importing image from MRI and measuring R2 value

```
>> namearray=dir;
>> c1=1; c2=1; c3=1;
for k = 3:62
if (mod(k,3)== 1)
ap = dicominfo(namearray(k).name);
te(c1,1)=double(ap.EchoTime);
lala = dicomread(namearray(k).name);
image(:,:,1,c1)=double(lala);
c1=c1+1;
end
if (mod(k,3)== 2)
lala = dicomread(namearray(k).name);
image(:,:,2,c2)=double(lala);
c2=c2+1;
end
if (mod(k,3)== 0)
```

```
lala = dicomread(namearray(k).name);
image(:,:,2,c3)=double(lala);
c3=c3+1;
end
clear ap; clear lala;
end
>> figure, plot(te)
>> size(image)
>> figure, imagesc(image(:,:,1,1))
>> colormap(gray)
>> figure, plot(te,squeeze(image(119,327,1,:)))
>> for k=1:20
rara = image(117:122,325:330,1,k);
signal(k,1)=mean(rara(:));
end
>> figure, plot(te,signal)
>> x = ones(19,2);
>> x(:,2)=te(2:20,1)/1000;
>> beta = (transpose(x)*x)^(-1)*transpose(x)*log(signal(2:20,1))
```